JGR Solid Earth

RESEARCH ARTICLE
10.1029/2018JB016487

Key Points:
- Early Jurassic subduction-related mafic intrusions in NE China show distinct geochemical compositions
- Both terrigenous and pelagic sediments contributed to mantle enrichments across the subduction zone
- The Paleo-Pacific subduction zone in NE China contained both oceanic and continental arcs

Supporting Information:
- Supporting Information S1
- Data Set S1

Correspondence to:
L. Zhao,
zhaoliang@gig.ac.cn

Citation:
Zhao, L., Guo, F., Fan, W., & Huang, M. (2019). Roles of subducted pelagic and terrigenous sediments in Early Jurassic mafic magmatism in NE China: Constraints on the architecture of Paleo-Pacific subduction zone. *Journal of Geophysical Research: Solid Earth*, *124*, 2525–2550. https://doi.org/10.1029/2018JB016487

Received 31 JUL 2018
Accepted 10 FEB 2019
Accepted article online 13 FEB 2019
Published online 15 MAR 2019

Roles of Subducted Pelagic and Terrigenous Sediments in Early Jurassic Mafic Magmatism in NE China: Constraints on the Architecture of Paleo-Pacific Subduction Zone

Liang Zhao[1], Feng Guo[1], Weiming Fan[1,2], and Miwei Huang[1,2]

[1]State Kay Laboratory of Isotope Geochemistry, Guangzhou Institute of Geochemistry, Chinese Academy of Sciences, Guangzhou, China, [2]University of Chinese Academy of Sciences, Beijing, China

Abstract The role of subducted sediments in arc magmatism has been widely documented. However, identifying the sedimentary provenance (e.g., pelagic vs. terrigenous) input in subduction systems is difficult because of the wide compositional range of sedimentary components and the complex magmatic evolution of arcs. Here we report zircon U-Pb-Hf-O isotopes and whole-rock elemental and Sr-Nd-Hf isotopic compositions of four Early Jurassic subduction-related mafic intrusions from the Yanbian area, NE China. These rocks show typical trace element and isotopic features of arc magmas. In combination with the published data, we discover two distinct elemental-isotopic arrays of the Early Jurassic mafic rocks across the arc magmatic belt. Such geochemical variations are mainly attributed to variable subducted sediment input into the mantle wedge instead of crustal contamination or assimilation during magmatic evolution. The mantle source for the southern Yanbian mafic rocks was enriched by addition of a crustal component dominated by terrigenous sediments, whereas that for the northern Lesser Hinggan-Zhangguangcai Range, mafic rocks was modified by another crustal component comprising mainly pelagic sediments. The results can be best interpreted if the southern part was a continental arc as opposed to an oceanic arc in the north, which is analogous to the modern Kamchatka-Honshu-Izu-Bonin-Mariana arc systems in the western Pacific. Our reconstructed architecture, based mainly on the geochemical data, further suggests that the Khanka-Jiamusi-Buleya Massif was probably sinistrally and northwardly displaced to the present position after Mesozoic subduction of the Paleo-Pacific Ocean.

Plain Language Summary Subducted sediments play an important role in generation of arc magmatism. However, the identification of the source (pelagic vs. terrigenous) of the sediments in subduction systems is difficult because of the wide compositional range of sedimentary components and the complex magmatic evolution of arcs. Here we carry out an integrated analysis of Sr-Nd-Hf-O isotopic and elemental compositions of subduction-related mafic intrusions across the Early Jurassic Paleo-Pacific subduction zone in NE China. The combined geochemical data from our and previous studies suggest that the southern Yanbian mafic rocks were generated by melting of a depleted mantle with input of a terrigenous sediment component, whereas the mafic rocks from the northern Lesser Hinggan-Zhangguangcai Range were derived from a depleted mantle modified by a pelagic sediment component. We thus propose that the Mesozoic subduction zone in NE China consisted of an intraoceanic arc in the northern segment and a continental arc in the southern part, as observed from the modern Kamchatka-Honshu-Izu-Bonin-Mariana arc systems in the western Pacific. Our study therefore provides a potential method to identify the provenance of the subducted sediments added into the subarc mantle, which may allow to reconstruct the architecture of paleo-subduction zones.

1. Introduction

Subduction zones are among the most important sites for mass and energy exchange between the Earth's mantle and crust and also the regions of crustal growth (Aizawa et al., 1999; Hawkesworth et al., 1993; Manning, 2004; Marini et al., 2005; McCulloch & Gamble, 1991; Scholl & von Huene, 2007; Tatsumi & Kogiso, 2003). At subduction zones, crustal materials such as altered oceanic crust and pelagic/terrigenous sediments are introduced into mantle (Elliott et al., 1997; Hanyu et al., 2006; Marschall & Schumacher, 2012; Tatsumi & Kogiso, 2003; Walowski et al., 2016). Melts and/or fluids

liberated from the subducted sediments interact with the overlying mantle wedge and facilitate melting of the mantle source to generate arc magmas (Cousens et al., 1994; Hermann & Spandler, 2008; Kessel et al., 2005; Macdonald et al., 2000; Marini et al., 2005; Marschall & Schumacher, 2012; Stolz et al., 1996; Tatsumi et al., 1986; Tatsumi & Kogiso, 2003). Petrological and geochemical studies indicate that the subduction-related magmas have compositions similar to those of the average continental crust but different from those of the mid-ocean ridge basalts (MORBs) and oceanic island basalts (OIBs). For instance, most arc basalts formed at convergent plate margins are marked by enrichments in Large Ion Lithophile Element (LILE) and Light Rare Earth Elements (LREE) and relative depletions in High Field Strength Element (HFSE) compared to MORBs and oceanic island basalts. A possible explanation is that arc magmas may inherit the geochemical characteristics of the sediments subducted into the mantle wedge (Cousens et al., 1994; Marini et al., 2005; Plank, 2005; Plank & Langmuir, 1993; Shimoda et al., 1998).

According to seismological and petrological data, two types of magmatic arcs can be identified in modern subduction zones. Continental arcs (e.g., the Andes arc) form when an oceanic plate is subducted beneath a continental plate, whereas oceanic arcs (e.g., the Izu-Bonin-Mariana arcs) form by subduction of an oceanic plate beneath another oceanic plate (Cao et al., 2017; Porritt et al., 2016). Because of the location distant from continental crust, sediments transported from the subducted slab into the mantle wedge are usually pelagic in oceanic arcs. In contrast, terrigenous sediments are predominant in continental arcs. However, some recent studies also show that the sedimentary components consist of both terrigenous and pelagic origins in most subduction zones. For instance, pelagic sedimentary rocks from the modern (e.g., the Izu-Bonin-Mariana arcs) and ancient oceanic arcs (e.g., oceanic arcs in the Arabian-Nubian Shield) also contain abundant old continental detritus (Chauvel et al., 2009; X. H. Li et al., 2018; Plank et al., 2007; Plank & Langmuir, 1998). Furthermore, both pelagic and terrigenous sediments display large range in their compositions (Chauvel et al., 2008, 2009; Lin, 1992; Plank et al., 2007; Plank & Langmuir, 1998). Accordingly, these complexities make it difficult to identify the provenance (pelagic vs. terrigenous) of the recycled sediments and to investigate the mechanisms through which the mantle wedges are enriched (e.g., Nichols et al., 1994; Plank, 2005; Rapp et al., 2008; Tollstrup & Gill, 2005).

A potential way to evaluate the contribution of subducted sediments (terrigenous or pelagic sediments) to the source of magmatic rocks produced in modern subduction zones is to use the distinct elemental and isotopic signatures of the two types of sediment. Hafnium is concentrated in zircon, while Nd is mainly concentrated in clay minerals. Thus, the coarser-grained terrigenous sediments have higher Hf/Nd and lower Lu/Hf ratios and nonradiogenic Hf isotopic compositions, whereas the finer-grained pelagic sediments usually have lower Hf/Nd and higher Lu/Hf ratios and more radiogenic Hf with time (Bayon et al., 2009; David et al., 2001; Marini et al., 2005; Plank & Langmuir, 1998; Vervoort et al., 1999, 2011). Theoretically, addition of sediments with different provenance into the mantle source will produce arc magmas with distinct elemental and isotopic compositions in Nd and Hf. However, in an ε_{Nd} versus ε_{Hf} diagram, most terrigenous sediments plot along or even above the terrestrial array (Chauvel et al., 2008, 2009; van de Flierdt et al., 2007; Vervoort et al., 1999, 2011). Since the evolution of Nd and Hf isotopes of terrigenous sediments depends largely on the source rock and deposition time, the decoupling between Hf and Nd isotopes of such sediments is much weaker than expected. The terrigenous sediments derived from the ancient terranes comprising mainly felsic protoliths such as the Himalaya sandstones would show less radiogenic Hf than Nd (Richards et al., 2005), whereas those derived from the young orogens or accretionary complex such as the southwest Japan have insignificant Hf-Nd isotopic decoupling (e.g., Hanyu et al., 2006; Okamura et al., 2016). In fact, most modern continental arc magmas plot along or above the terrestrial array in the ε_{Nd} via ε_{Hf} diagram, suggesting that the time for the transportation and deposition of terrigenous sediments is not enough to lead to accumulate more radiogenic Nd than Hf.

In contrast with the degree of Hf-Nd isotopic decoupling, the differences in some elements and elemental ratios between the pelagic and terrigenous sediments are more obvious and time-independent such as Lu/Hf, Hf/Nd, and Th/La. These elemental imprints can be alternative fingerprints to evaluate the contribution of subducted sediments with different provenance to the mantle source for the arc igneous rocks (e.g., Churikova et al., 2001; Cousens et al., 1994; Handley et al., 2011; Lin, 1992; Marini et al., 2005; Marschall & Schumacher, 2012; Münker et al., 2004; J. A. Pearce et al., 1999; Portnyagin et al., 2005; Shimoda et al., 1998; Turner et al., 2009; Walowski et al., 2016).

NE China, as a part of the circum-Pacific tectonic domain, is characterized by widespread Phanerozoic granitoids with subordinate Mesozoic mafic intrusions (Guo et al., 2015; Wu et al., 2011; Yu et al., 2012). However, typical Mesozoic arc basalts are absent in this ancient subduction zone due to extensive uplifting, unroofing, and erosion. Alternatively, their coeval intrusive counterparts (e.g., gabbro and diorite) were partly preserved and may provide potential information on the architecture and evolution of this paleo-subduction zone. Previous studies on the Early Jurassic mafic intrusions suggested that they were generated by melting of a mantle wedge that had been metasomatized by components derived from subducting sediments (Guo et al., 2015; Yu et al., 2012). Nevertheless, the provenance of the sediments subducted along the arc magmatic belt and the architecture of the subduction zone are still poorly constrained.

Here we present in situ zircon U-Pb-Hf-O isotopic compositions and whole-rock elemental and Sr-Nd-Hf isotopic results from four Early Jurassic mafic intrusions from the Yanbian area in NE China. By integration with the sedimentary records from the subduction-accretionary complexes and geochemical comparison with the contemporaneous mafic rocks in the Lesser Hinggan-Zhangguangcai Range (LHZR)—the northern part of this arc magmatic belt, these new data provide insights into the provenance of the subducted sediments associated with the Mesozoic subduction of the Paleo-Pacific Ocean. The combined results enable us to outline the architecture of the Early Jurassic subduction zone in NE China and provide a potential method to reconstruct the structure of ancient subduction zones by identifying the provenance of subducted sediments recorded in arc magmas.

2. Geological Background and Sample Description

The Central Asian Orogenic Belt (CAOB) is a giant accretionary orogen situated between the Siberian Craton in the north and the North China and Tarim Cratons in the south (Figure 1a). NE China forms the eastern segment of the CAOB. It comprises several microblocks including the Wandashan, Khanka, Jiamusi, Bureya, and Hinggan Massifs from east to west (Guo et al., 2010; Maruyama et al., 1989; Wu et al., 2000; Xiao et al., 2003; B. Xu et al., 2015; Figure 1b). This region has undergone two main stages of tectonic evolution (Guo et al., 2015; Maruyama et al., 1989; Wu et al., 2000, 2011): subduction and closure of the Paleo-Asian Ocean in the Paleozoic and westward subduction and accretion of the Paleo-Pacific Ocean since the Early Jurassic.

The Mesozoic subduction of the Paleo-Pacific Ocean has been documented in the subduction-accretionary complex along the N-S-trending LHZR-Yanbian arc magmatic belt (Figure 1c). The Heilongjiang Complex, considered as an accretionary complex, lies parallel to this arc magmatic belt (Ge et al., 2016; Zhou et al., 2009; Zhou & Li, 2017; Figure 1c). It consists of mafic-ultramafic rocks, quartz-feldspathic schists, and radiolarian cherts and has experienced blueschist-facies metamorphism (Zhou et al., 2009; Zhou & Li, 2017). The Raohe Complex, located in the northern segment of the belt, is composed of mafic intrusions and lavas and deep-oceanic radiolaria-bearing silicalite (Cheng et al., 2006; Zhou et al., 2014). In addition, the Kaishantun ophiolitic mélange, located in the Yanbian area at the southern segment of the belt, consists predominantly of a suite of mafic-ultramafic rocks and terrigenous sediments (e.g., nagelfluh; Shao & Tang, 1995). The sedimentary records preserved in these subduction-accretionary complexes indicate that the amount of pelagic sediments increased from south to north in the belt. Mesozoic magmatism (mainly Triassic-Jurassic granitoids) was extensive in association with the subduction of the Paleo-Pacific Ocean (Wu et al., 2011). The mafic intrusions are distributed heterogeneously from north to south among the LHZR-Yanbian arc magmatic belt (Figure 1c).

The Yanbian area is located at the junction of China, Russia, and Korea and about 100-km west of the Japan Sea. It is situated between the North China Craton to the south and the Buleya-Jiamusi-Khanka Massifs to the northeast (Figures 1b and 1c). Phanerozoic granitoids are widespread and occupy about 70% of this region (Wu et al., 2000, 2011; Figure 2). These granitoids were emplaced from the Permian (285 Ma) to Early Cretaceous (112 Ma) with a peak at 210–115 Ma (Wu et al., 2011; Y. B. Zhang et al., 2004). Compared to the voluminous granitoids, the Early Jurassic mafic intrusions are distributed heterogeneously in the Yanbian area and its adjacent regions (e.g., the LHZR in the northern part of the magmatic belt). The mafic intrusions consist of hornblende-bearing norite, gabbro, diorite, and mafic dykes (BGMRJL, 1989). Formation of these Early Jurassic (187–182 Ma) mafic intrusive complexes in the Yanbian area and LHZR

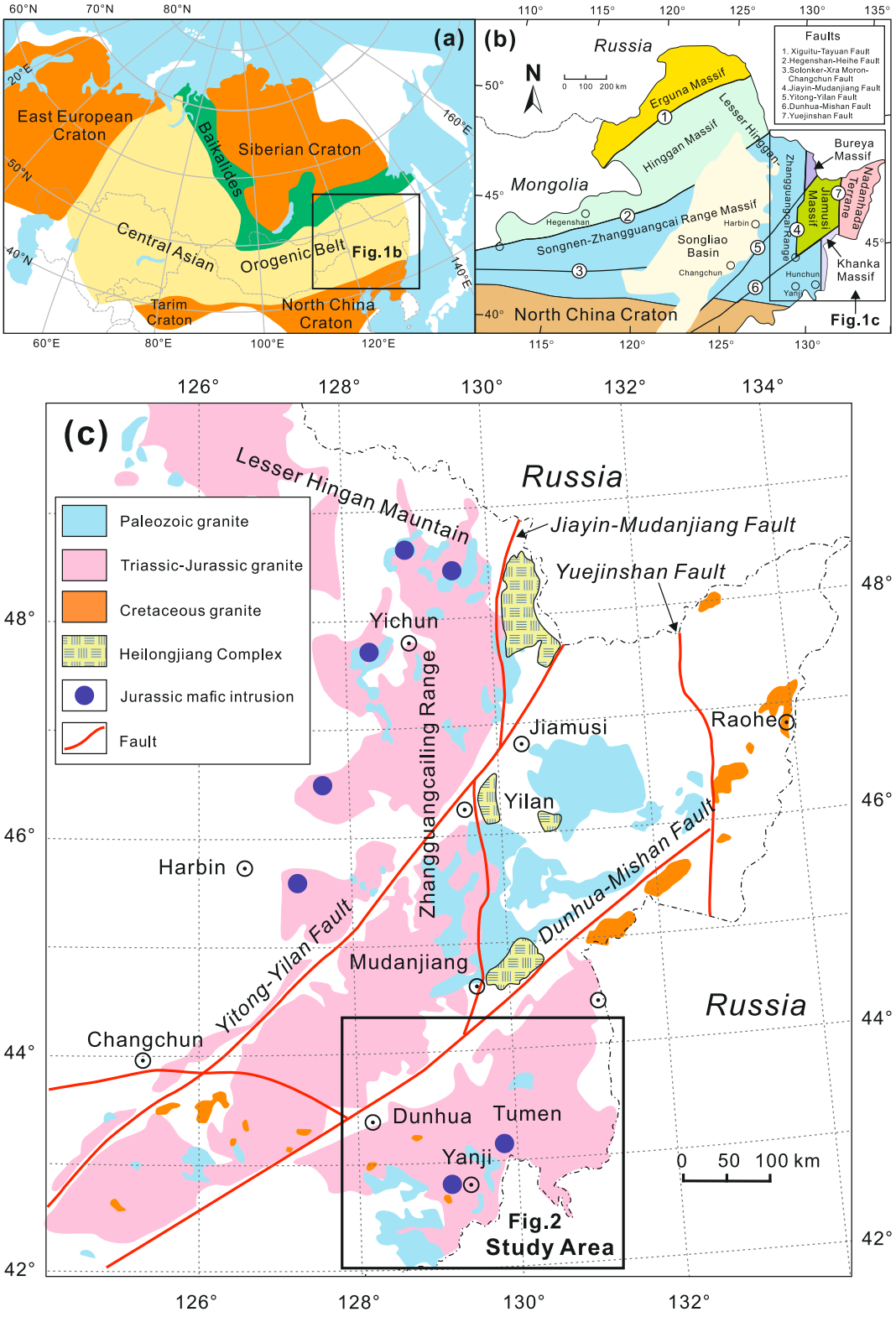

Figure 1. (a) Simplified tectonic map of the Central Asian Orogenic Belt (modified after Sengör et al., 1993, and Windley et al., 2007) and (b) NE China (modified after Wu et al., 2007) and (c) distribution of Phanerozoic granitoids, mafic intrusions, and Heilongjiang Complex in NE China (after Wu et al., 2011, and Yu et al., 2012).

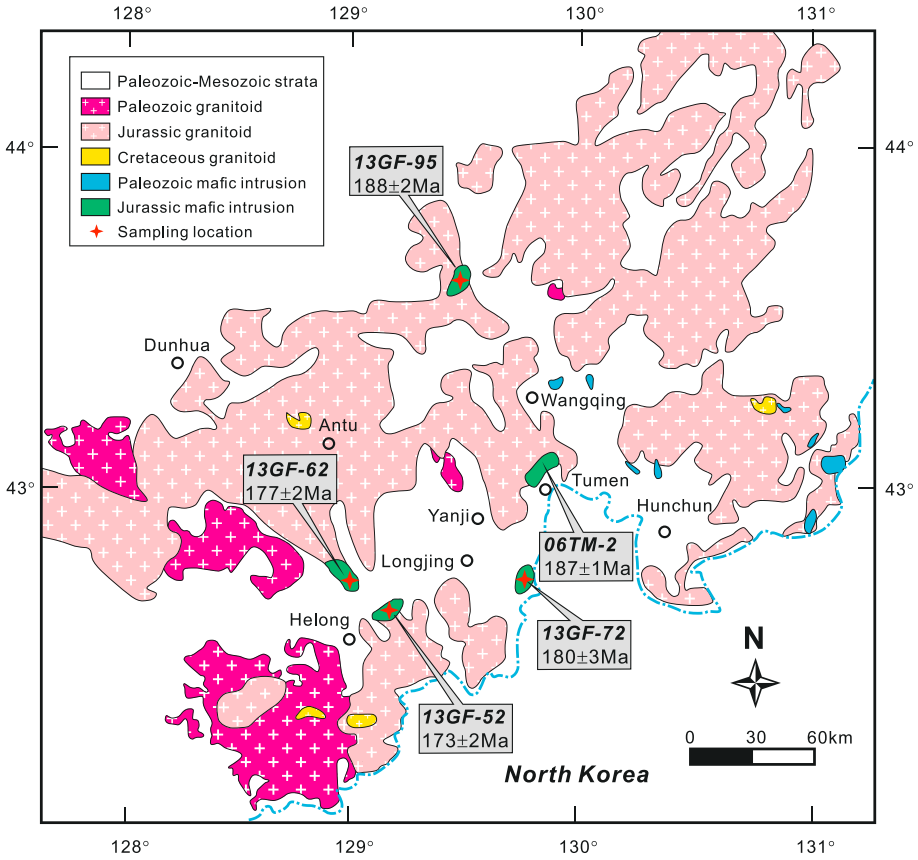

Figure 2. A geological map of the Yanbian area, showing the distributions of the Early Jurassic mafic intrusions (modified after BGMRJL, 1989). 06TM-2 is from Guo et al. (2015).

has previously been attributed to westward subduction of the Paleo-Pacific Ocean beneath the Eurasian Continent (Guo et al., 2015; Yu et al., 2012).

The mafic rocks in this study are all diorites and were sampled from four localities, including Shacongdingzi, Shangnan, Kaishantun, and Chunyang in the Yanbian area (Figure 2). The locations, detailed occurrence, and petrologic description are summarized below.

1. The Shacongdingzi diorite is located at about 40 km northeast to Helong City. The diorite is fine- to medium-grained and mainly comprises plagioclase (50–60%), hornblende (30–40%), clinopyroxene (~5%), and biotite (~5%), with accessory zircon, apatite, and magnetite (Figures 3a–3c).
2. The Shangnan diorite is located at about 50 km north to Helong City. The diorite is fine- to medium-grained and contains plagioclase (55–60%), hornblende (40–45%), clinopyroxene (~2%), and biotite (~3%), with accessory minerals such as zircon, apatite, and magnetite (Figure 3d).
3. The Kaishantun diorite is located at about 45 km east to Longjing City. The rocks are gray, medium- to coarse-grained, and contain plagioclase (50–55%) and hornblende (45–50%), with subordinate clinopyroxene (~2%) and accessory zircon, apatite, and magnetite (Figure 3e).
4. The Chunyang diorite is located at around 90 km northwest to Wangqing City. The rocks are medium- to coarse-grained and mainly consist of plagioclase (~60%) and hornblende (~40%), with accessory zircon, magnetite, and apatite (Figure 3f).

3. Analytical Methods

3.1. In Situ Zircon U-Pb-Hf-O Isotope Analyses

Zircons were extracted from four samples (13GF-52, 13GF-62, 13GF-72, and 13GF-95) using conventional heavy-liquid and magnetic separation techniques. Zircon grains were then handpicked under a binocular

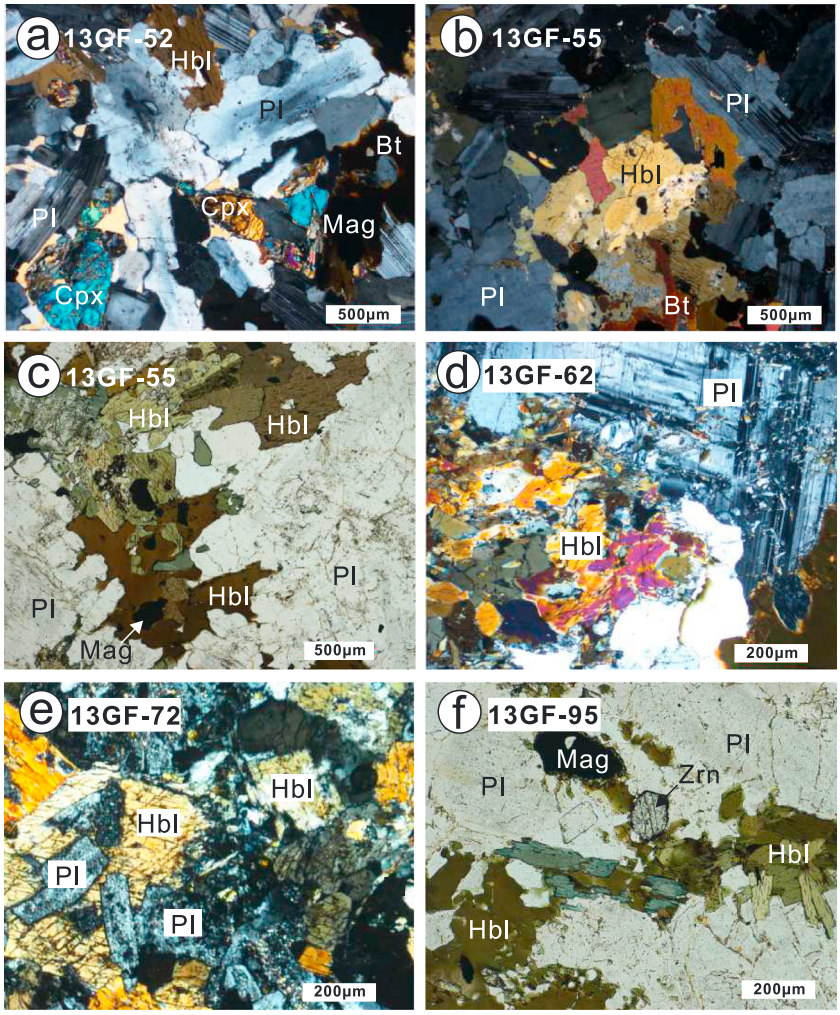

Figure 3. Photomicrographs of mafic intrusions from the Yanbian area, NE China. (a), (b), (d), and (e) are in cross-polarized light, while (c) and (f) are in plane-polarized light. Mineral abbreviations are after Whitney and Evans (2010). Cpx = clinopyroxene; Pl = plagioclase; Hbl = hornblende; Bt = biotite; Mag = magnetite; Zrn = zircon.

microscope, mounted in epoxy resin discs together with zircon standards TEMORA, Mud Tank, Qinghu and Penglai, and polished to about half thickness for analysis. Cathodoluminescence (CL) images of analyzed zircons were obtained using a JEOL JXA-8100 microprobe.

Zircon U-Pb dating and trace element analyses were conducted using laser-ablation multicollector inductively coupled plasma mass spectrometry at the Guangzhou Institute of Geochemistry (GIG), Chinese Academy of Sciences (CAS). Detailed analytical procedures were described in C. Y. Li et al. (2012). The laser-ablation multicollector inductively coupled plasma mass spectrometry (ICP-MS) system consists of an Agilent 7500a ICP-MS coupled with a Resonetic RESOLution M-50 ArF-Excimer laser source (λ = 193 nm). The conditions were 80-mJ laser energy and repetition rate of 10 Hz with a spot size of 63 μm in diameter and ablation time of 40 s. The ablated aerosol was carried to the inductively coupled plasma source by helium via a Squid system to smooth the signals. NIST610 (Gao et al., 2002; N. J. G. Pearce et al., 1997) and zircon standard TEMORA (Black et al., 2003) were used as external calibration standards and ^{29}Si as the internal standard. Each block of five unknowns was bracketed by analyses of standards. Quantitative calibration for zircon isotope ratios and trace elements was performed by ICPMSDataCal 7.0 (Y. S. Liu et al., 2008, 2010). Weighted mean calculations of zircon age and concordia diagrams were made using Isoplote program (version 3.0; Ludwig, 2003).

In situ zircon oxygen isotopes were analyzed in the same grains that were dated for U-Pb isotopes, using a Secondary Ion Microprobe Spectrometer Cameca IMS 1280 at the Institute of Geology and Geophysics, CAS. The Cs^+ primary ion beam was accelerated at 10 kV with an intensity of ca. 2 nA. The ellipsoidal spot is about 20 μm × 30 μm in size. A normal-incidence electron flood gun was used to compensate for sample charging during analysis. Secondary ions were extracted with a −10-kV potential. Oxygen isotopes were measured in multicollector mode using teo off-axis Faraday cups with each analysis consisting of 4 × 20 cycles of ion counting. Internal precision of a single analysis was better than 0.2‰ for $^{18}O/^{16}O$. Oxygen isotope results are reported in the conventional $\delta^{18}O$ notation and standardized to Vienna Standard Mean Ocean Water (VSMOW; Baertschi, 1976). The instrumental mass fractionation factor was corrected using zircon standard 91500 with $(\delta^{18}O)_{VSMOW} = 9.9‰$ (Wiedenbeck et al., 2004). Detailed description of working conditions and analytical procedures were reported by X. H. Li et al. (2010) and Tang et al. (2015).

In situ zircon Lu-Hf isotopes were measured using a Neptune multicollector ICP-MS equipped with a 193-nm laser ablation system at the Institute of Geology and Geophysics, CAS. The analytical technique and calibration methods were described by Wu et al. (2006) and X. H. Li et al. (2010). Lutetium-Hf isotope measurements were obtained on the same spots that were previously analyzed for oxygen isotope. Laser ablation operating conditions include an ablation time of 26 s, repetition rate of 10 Hz, laser beam energy density of 10 J/cm^2, and ablation spot diameter of 63 μm. Measured $^{176}Hf/^{177}Hf$ ratios were normalized to $^{179}Hf/^{177}Hf = 0.7325$. The single zircon U-Pb ages were used to calculate $\varepsilon_{Hf}(t)$ values with the parameters including ^{176}Lu decay constant of $\lambda = 1.867 \times 10^{-11}$ year^{-1} (Söderlund et al., 2004), chondritic values of $^{176}Hf/^{177}Hf = 0.282785$ and $^{176}Lu/^{177}Hf = 0.0336$ (Bouvier et al., 2008).

A comprehensive data set of the in situ zircon U-Pb, Lu-Hf, and O isotope results is presented in Data Set S1 in the supporting information.

3.2. Whole-Rock Major and Trace Elements and Sr-Nd-Hf Isotope Analyses

Samples for whole-rock major and trace elements and Sr-Nd-Hf isotope analyses were crushed, and the fresh chips were selected and washed in 0.05 N HCl and purified water. The cleaned chips were then powdered in an agate mortar to less than 200 meshes. Whole-rock major oxides were analyzed by X-ray fluorescence spectrometry on fused glass pellets at the GIG, CAS. The analytical precisions for major elements were better than 2%.

Trace element analyses were carried out using ICP-MS at Institute of Geochemistry, CAS. Detailed analytical procedures were described by Qi et al. (2000). About 50-mg powders digested in 1-ml HF and 0.5-ml HNO_3 in Teflon beakers sealed in screw-top stainless steel bombs at 190 °C for 12 hr. The analytical precision is generally better than 5% for elements with concentrations >200 ppm and 5–10% for concentrations <200 ppm. The results of whole-rock major and trace elements composition are listed in Data Set S2.

Strontium and Nd isotopes were determined using a Neptune multicollector ICP-MS at the GIG, CAS. Detailed description of the analytical procedures was reported by Wei et al. (2002) and Liang et al. (2003). Powders were dissolved in HF-$HClO_4$ at 150 °C for a week. Strontium and the Rare Earth Element (REE) were separated using ion exchange columns with a 0.1% HNO_3 eluant, and Nd fractions were further separated using HDEHP-coated Kef columns with a 0.18 N HCl eluant. The NBS SRM 987 and JNDi-1 standards were used as monitors of the detector efficiency drift of the instrument for Sr and Nd isotopes, respectively. Measured $^{87}Sr/^{86}Sr$ and $^{143}Nd/^{144}Nd$ ratios were normalized to $^{86}Sr/^{88}Sr = 0.1194$ and $^{146}Nd/^{144}Nd = 0.7219$, respectively. The reported $^{87}Sr/^{86}Sr$ and $^{143}Nd/^{144}Nd$ ratios were adjusted to the NBS SRM 987 standard with an average of $^{87}Sr/^{86}Sr = 0.710249$ (2σ, $n = 14$) and the JNDi-1 standard with an average of $^{143}Nd/^{144}Nd = 0.512093 \pm 5$ (2σ, $n = 14$), respectively. The U.S. Geological Survey standard BHVO-2 was used as the standard to monitor the instrumental performance for Sr and Nd isotopes and yielded an average of $^{87}Sr/^{86}Sr = 0.703489 \pm 6$ (2σ, $n = 12$) and an average of $^{143}Nd/^{144}Nd = 0.512981 \pm 5$ (2σ, $n = 12$).

Hafnium isotope analyses were conducted using a Finnigan Neptune multicollector ICP-MS system in the GIG, CAS. Detailed analytical procedures were described by X. H. Li et al. (2006). For Hf isotope analyses, mixtures of 0.5-g whole-rock powders and 1.0-g $Li_2B_4O_7$ were first fused in Pt crucibles at 1,250 °C for 15 min in a high-frequency furnace. The glasses (~400 mg) were then dissolved in 2 N HCl. Hf fractions were separated using a modified ion exchange single-column with Ln-Spec resin. Measured $^{176}Hf/^{177}Hf$ ratios

were normalized to $^{179}Hf/^{177}Hf = 0.7325$. The reported $^{176}Hf/^{177}Hf$ ratios were adjusted to the JMC-475 standard (0.282160 ± 7, 2σ). During Hf isotope analyses, the BHVO-2 standard gave an average of $^{176}Hf/^{177}Hf = 0.283097 \pm 12$ (2σ), which is consistent with the recommended value (Weis et al., 2005). The whole-rock Sr-Nd-Hf isotopic compositions are listed in Data Set S3.

4. Results

4.1. Zircon U-Pb Ages and Hf-O Isotopic Compositions

4.1.1. Shacongdingzi Diorite

Zircons separated from diorite sample 13GF-52 are euhedral and prismatic and approximately 150 to 400 μm long with length/width ratios of 2.0–3.0. Most zircon grains show well-developed oscillatory zoning in CL images (Figure S1a) and high Th/U ratios (0.47–1.43), indicating a magmatic origin. Nineteen U-Pb isotope analyses on concordant zircons yield a mean weighted $^{206}Pb/^{238}U$ age of 173 ± 2 Ma (MSWD = 2.2, n = 17; Figure S2a), which is interpreted to reflect an Early Jurassic emplacement age for the Shacongdingzi diorite.

Sixteen of those zircon grains were analyzed for Hf and O isotopic compositions. They give a narrow $\varepsilon_{Hf}(t)$ range between +1.0 and +4.0 and a T_{DM} range of 825–939 Ma. The O isotopic compositions of zircons show a narrow $\delta^{18}O_{VSMOW}$ range between 6.2‰ and 6.8‰, higher than that of mantle zircon of $\delta^{18}O_{VSMOW} = 5.3 \pm 0.3$‰ (Valley, 2003).

4.1.2. Shangnan Diorite

Zircons from diorite sample 13GF-62 are also euhedral, transparent, and approximately 200–400 μm long and 100–200 μm wide with length/width ratios of 2.0–3.0. Most zircon grains exhibit well-developed oscillatory zoning in CL images (Figure S1b) and have high Th/U ratios (0.65–1.09), suggesting a magmatic origin. Sixteen U-Pb analyses of concordant zircons yield a mean weighted $^{206}Pb/^{238}U$ age of 177 ± 2 Ma (MSWD = 1.5, n = 16; Figure S2b), which is considered as the crystallization age for the Shacongdingzi diorite.

Hafnium and O isotopic analyses were carried out on 13 of those zircon grains. The zircon grains have an $\varepsilon_{Hf}(t)$ range between +1.6 and +5.3 and a T_{DM} range of 756–975 Ma. The zircons have $\delta^{18}O_{VSMOW}$ values ranging from 5.8‰ to 6.6‰, which is slightly higher than that of mantle zircon (Valley, 2003).

4.1.3. Kaishantun Diorite

Zircons from diorite sample 13GF-72 are relatively short (60–150 μm long) with length to width ratios of approximately 2:1. Most of the crystals are euhedral with concentric oscillatory zoning (Figure S1c). Twenty-one analyses on zircons yield relatively high Th/U ratios (0.33–1.62). Four zircon grains yield Paleozoic apparent $^{206}Pb/^{238}U$ ages of 401, 407, 431, and 445 Ma (Figure S2c), similar to the early Paleozoic tonalite in the Yanbian area (Z. W. Wang, Pei, et al., 2016). Three zircon grains give Triassic U-Pb ages (207, 213, and 251 Ma), and discordant Middle Jurassic U-Pb ages (160 and 163 Ma) are obtained from two grains. The concordant zircon U-Pb ages are similar to ages from the Paleozoic basement rocks of the region and to the Early Mesozoic granitoids from the Khanka Massif (K. Liu, Zhang, Wilde, Zhou, et al., 2017), respectively. The remaining 11 U-Pb isotopic analyses define a weighted mean $^{206}Pb/^{238}U$ age of 180 ± 3 Ma (MSWD = 3.6, n = 11; Figure S2c), which is interpreted as the emplacement age for the Kaishantun diorite.

The four Paleozoic zircon grains show an $\varepsilon_{Hf}(t)$ range between −6.7 and −8.4 and a T_{DM} range from 1,411 to 1,467 Ma. These zircons yield a $\delta^{18}O_{VSMOW}$ range between 7.7‰ and 9.0‰. The main group of magmatic zircons (180 Ma) display a large $\varepsilon_{Hf}(t)$ range between +0.2 and +9.7 and a T_{DM} range from 591 to 957 Ma. They show a $\delta^{18}O_{VSMOW}$ range from 5.6‰ to 7.1‰. The Hf and O isotopic compositions of these magmatic zircons are distinct from those of the inherited Paleozoic zircons.

4.1.4. Chunyang Diorite

Zircons from diorite sample 13GF-95 are euhedral, prismatic, 100 to 250 μm in length with a range of length/width ratio from 1.2 to 2.5, and show oscillatory zoning (Figure S1d). They have high Th/U ratios (0.29–0.95) consistent with a magmatic origin. A total of 27 analyses on concordant zircons yield a weighted mean $^{206}Pb/^{238}U$ age of 188 ± 2 Ma (MSWD = 2.7, n = 27; Figure S2c), similar to that of the Tumen mafic intrusive complexes in the Yanbian area and other mafic intrusions in the LHZR (Guo et al., 2015; Yu et al., 2012).

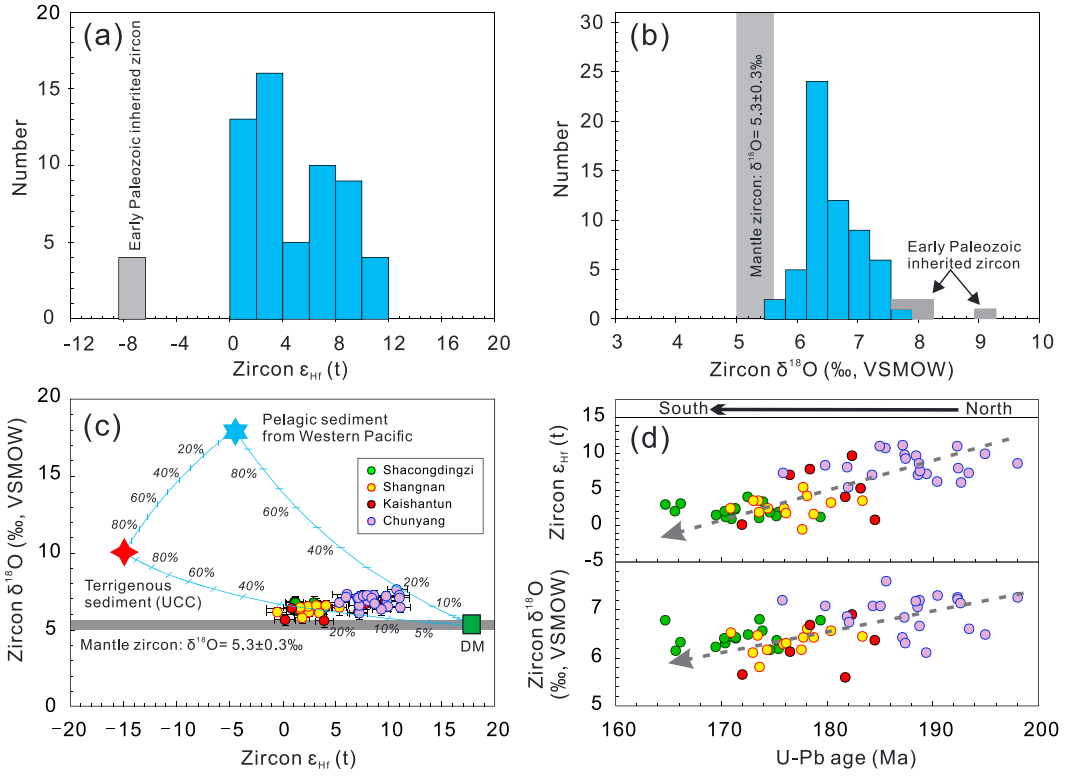

Figure 4. (a) $\varepsilon_{Hf}(t)$ and (b) $\delta^{18}O_{VSMOW}$ isotope histograms; (c) $\delta^{18}O_{VSMOW}$ versus $\varepsilon_{Hf}(t)$ diagrams of zircon; and (d) relationship between zircon U-Pb age and Hf and O isotopes of the Yanbian mafic intrusions. Terrigenous sediment is represented by the compositions of average upper continental crust (UCC), pelagic sediment is represented by pelagic clays from the western Pacific (W. Pacifc), and depleted mantle in NE China is estimated from the mafic components of the Hegenshan ophiolite suite and the Dashizhai arc basalts in Inner Mongolia (Guo et al., 2009; Miao et al., 2008). Hf-O isotopic compositions of end-member components used in the modeling are the following: (1) depleted mantle has $\varepsilon_{Hf}(t) = +18$ (Guo et al., 2009; Miao et al., 2008) and $\delta^{18}O_{VSMOW} = 5.25$ (Valley, 2003); (2) terrigenous sediment (UCC) has $\varepsilon_{Hf}(t) = -15$ (Chauvel et al., 2014) and $\delta^{18}O_{VSMOW} = 10$ (Bindeman, 2008; Eiler, 2001); and (3) pelagic sediment from Western Pacifc has $\varepsilon_{Hf}(t) = -4.5$ (J. A. Pearce et al., 1999; Woodhead, 1989) and $\delta^{18}O_{VSMOW} = 18$ (Clayton et al., 1972; Woodhead, 1989). Assumed proportions of Hf concentration of terrigenous sediment and pelagic sediment to depleted mantle are 3:1 and 2:1, respectively. VSMOW = Vienna Standard Mean Ocean Water.

Twenty-two of those zircon grains were analyzed for their Hf and O isotopes. They have an $\varepsilon_{Hf}(t)$ range between +5.3 and +11.1 and a T_{DM} range from 539 to 751 Ma. These zircons yield a narrow $\delta^{18}O_{VSMOW}$ range between 6.1‰ and 7.6‰, higher than that of mantle zircon.

In summary, the Yanbian mafic intrusions were formed between 188 and 173 Ma, which is roughly equivalent to those of the mafic intrusions in the N-S-trending LHZR-Yanbian belt to the north (Guo et al., 2015; Yu et al., 2012). In addition, the emplacement ages of the mafic rocks in the Yanbian area becomes younger from north to south (Figure 2). Zircons from the Yanbian mafic intrusions also show a large $\varepsilon_{Hf}(t)$ variation from +0.2 to +11.1 and generally display higher $\delta^{18}O_{VSMOW}$ values (5.6–7.6‰) than mantle zircons (Figures 4a and 4b). The zircon Hf-O isotopic array yields a trend of mixing between a juvenile component with mantle-like $\delta^{18}O_{VSMOW}$ and MORB-like $\varepsilon_{Hf}(t)$ and a recycled crustal component composed both terrigenous and pelagic sediments that have higher $\delta^{18}O_{VSMOW}$ and negative $\varepsilon_{Hf}(t)$ (Figure 4c). Furthermore, the zircon $\delta^{18}O_{VSMOW}$ and $\varepsilon_{Hf}(t)$ values tend to decrease simultaneously with the youthening of emplacement from north to south (Figure 4d).

Inherited zircons from the Kaishantun pluton, with U-Pb ages from 445 to 207 Ma (Figure S2c), display much less radiogenic Hf ($\varepsilon_{Hf}(t) = -8.4$ to -6.7) and higher $\delta^{18}O_{VSMOW}$ (7.7–9.0‰) than the magmatic zircons from the same sample. The combined Hf-O isotopic compositions of these inherited zircons clearly reflect the involvement of crustal material, perhaps of sedimentary origin (Figures 4c and 4d).

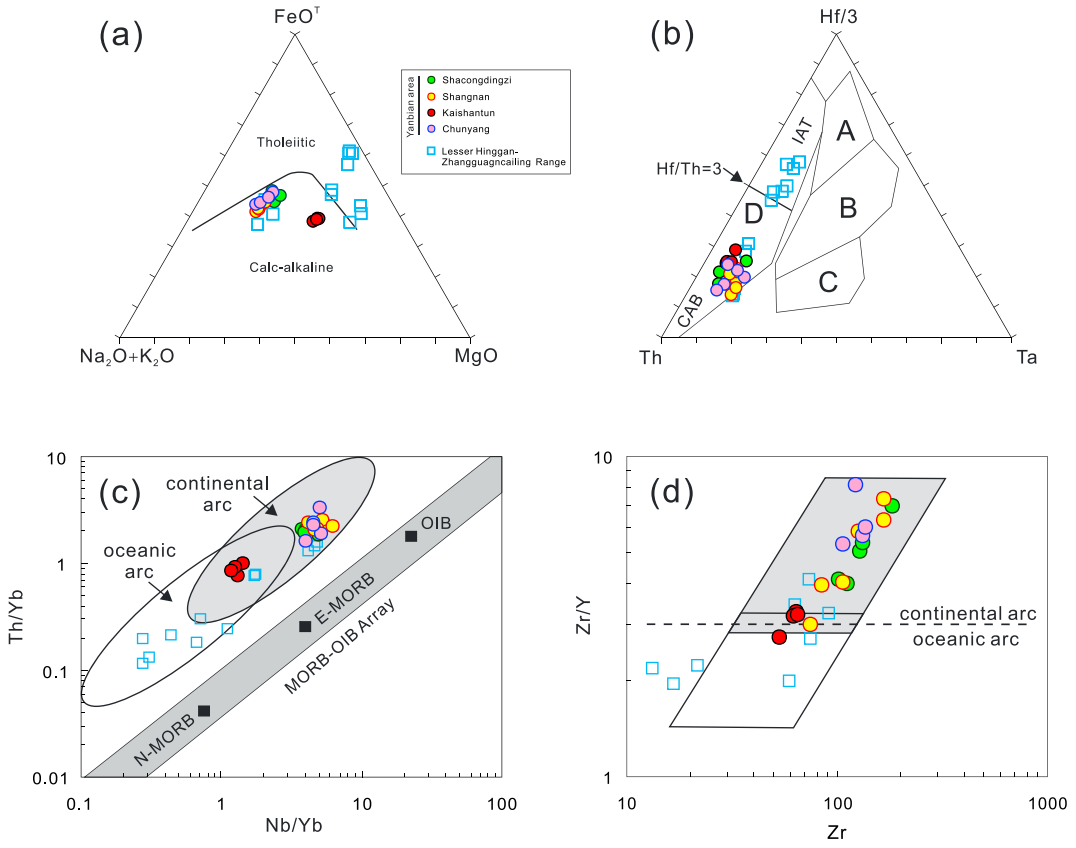

Figure 5. (a) AFM ternary (Irvine & Baragar, 1971), (b) Hf/3-Th-Ta (Wood, 1980), (c) Th/Yb versus Nb/Yb (J. A. Pearce, 2014), and (d) Zr/Y versus Zr (J. A. Pearce, 1983) plot for the Early Jurassic Yanbian mafic intrusions and contemporaneous mafic-ultramafic intrusive rocks in NE China. Data for mafic intrusive rocks from the Lesser Hinggan-Zhangguangcai Range is from Yu et al. (2012). In (b), the fields are the following: (A) N-type MORB; (B) E-type MORB and within plate tholeiites; (C) alkaline within-plate basalts; and (D) volcanic-arc basalts. In (D), the CAB and IAT are separated by a Hf/Th ratio of 3. MORB = mid-ocean ridge basalt; IOB = oceanic island basalt; CAB = calc-alkaline basalt; IAT = island-arc tholeiite.

4.2. Whole-Rock Major and Trace Elements

The Early Jurassic mafic rocks show large variations in SiO_2 (51.0–57.3 wt%), MgO (2.4–7.6 wt%), Fe_2O_3 (6.6–9.2 wt%), and $Mg^{\#}$ (41–63, Mg# = 100 × Mg / (Mg + Fe)). In a K_2O-SiO_2 diagram, most of the samples also plot in the field of medium-K calc-alkaline series with subordinate samples in the field of high-K calc-alkaline series (Figure S3). By comparison, the contemporaneous mafic rocks (mainly gabbros) in the LHZR generally have lower CaO, Fe_2O_3, MgO, and Mg# contents (Figure S3; Yu et al., 2012). On the $(Na_2O + K_2O)$-FeO^T-MgO (AFM) and Hf/3-Th-Ta diagrams, the Yanbian diorites plot within the calc-alkaline field, while the mafic rocks in the LHZR mainly plot in the field of tholeiitic series (Figures 5a and 5b). Furthermore, on the Th/Yb versus Nb/Yb and Zr/Y versus Zr discrimination diagrams (J. A. Pearce, 1983, 2014), all Yanbian mafic intrusions fall into the fields of continental arc, whereas the mafic intrusions from the LHZR fall into the fields of oceanic arc (Figures 5c and 5d).

On the primitive mantle-normalized incompatible element abundance diagrams (Figures 6a–6d), the Yanbian mafic rocks exhibit enrichments of LILE (e.g., Rb, Ba, K, and Sr) and LREE, and depletions in HFSE (e.g., Nb, Ta, and Ti), as observed in most arc magmas (J. A. Pearce & Peate, 1995; Shinjo et al., 1999). These mafic rocks show subparallel chondrite-normalized REE patterns, characterized by variable enrichment of LREE relative to HREE ($(La/Yb)_N$ = 3.5–9.2, *N* denotes chondrite normalization) and Eu anomalies (Eu/Eu^* ($2 \times Eu_{CN}/(Sm_{CN} + Gd_{CN})$) = 0.83–1.19, Figures 6e–6h).

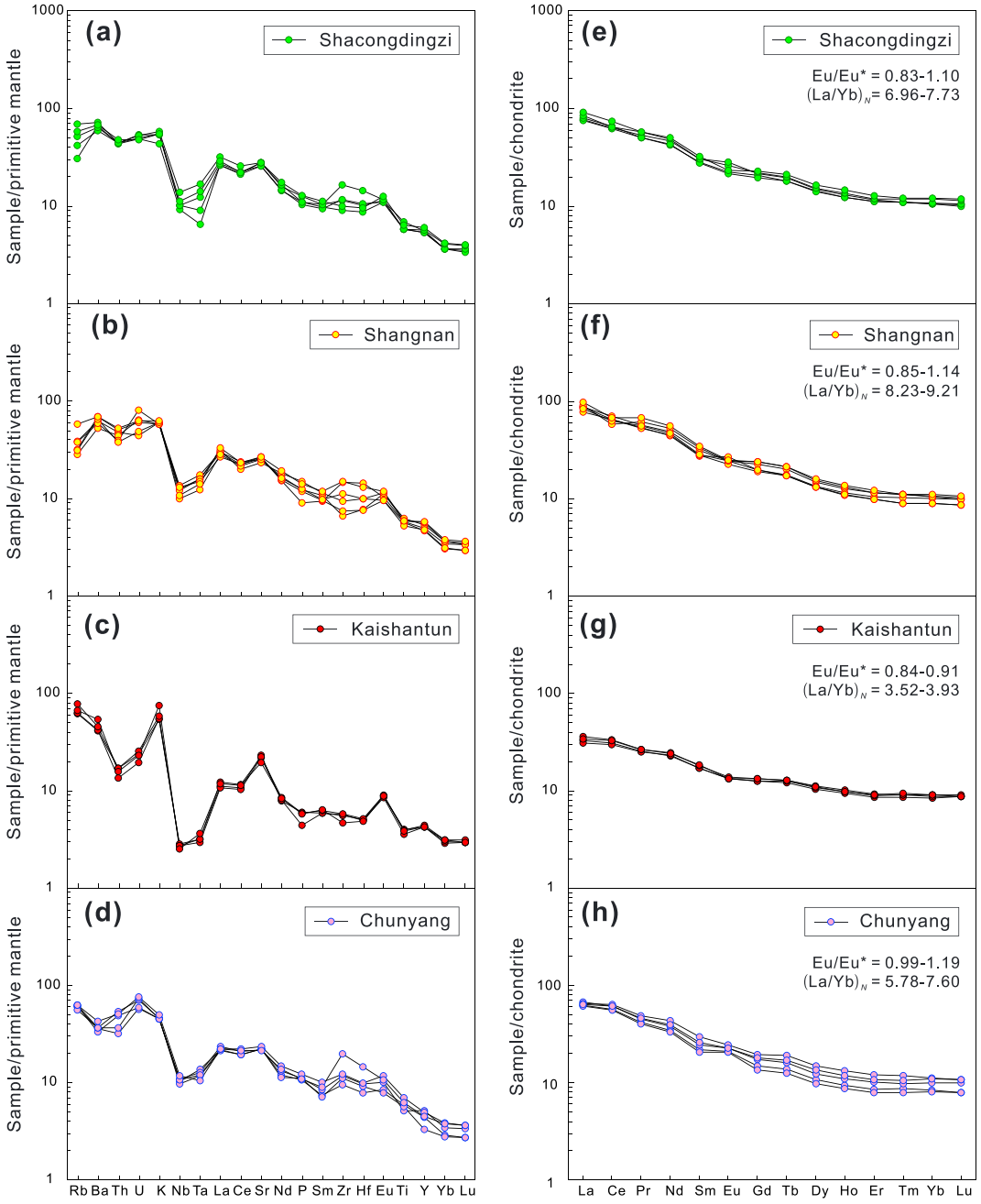

Figure 6. (a–d) Primitive mantle normalized trace element diagrams and (e–h) chondrite normalized REE patterns for the Yanbian mafic intrusions. Primitive mantle and chondrite normalization values are from Sun and McDonough (1989).

4.3. Whole-Rock Sr-Nd-Hf Isotopes

The four diorite plutons in the Yanbian area show relatively large Sr-Nd-Hf isotopic variations (Data Set S3 and Figure 7), although the isotopic ranges are quite narrow for the samples collected within each pluton. Four samples at Shacongdingzi display a narrow range of initial $^{87}Sr/^{86}Sr(i)$ from 0.7053 to 0.7054, an $\varepsilon_{Nd}(t)$ range from −1.8 to −2.3, and an $\varepsilon_{Hf}(t)$ range from +1.2 to +2.0. Three samples from Shangnan have quite similar Sr-Nd-Hf isotopic composition compared to those of the Shacongdingzi diorite, with $^{87}Sr/^{86}Sr(i) = 0.7054$ to 0.7055, $\varepsilon_{Nd}(t) = -1.2$ to 1.0, and $\varepsilon_{Hf}(t) = +2.5$ to +2.7. Four samples at Chunyang show a uniform and lower initial $^{87}Sr/^{86}Sr(i)$ of 0.7046–0.7048 and higher $\varepsilon_{Nd}(t)$ (+2.1 to +2.5) and $\varepsilon_{Hf}(t)$ (+7.6 to +9.0) than those of the Shacongdingzi and Shannan dioritic intrusions. Compared with the other

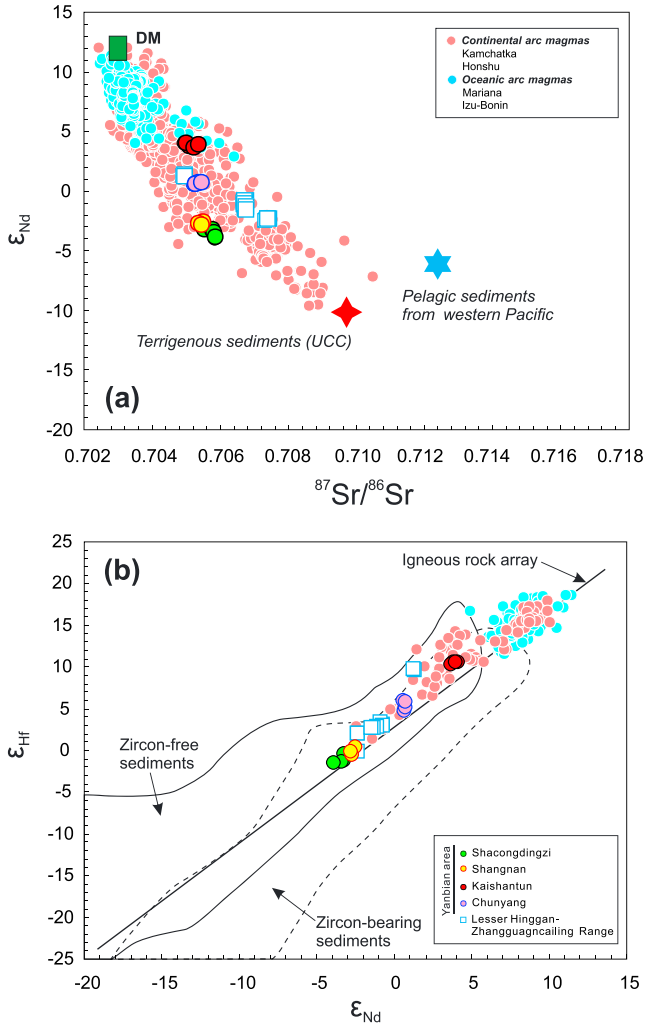

Figure 7. (a) Sr-Nd and (b) Hf-Nd isotope diagrams for the Yanbian mafic intrusions and contemporaneous mafic-ultramafic intrusive rocks from the Lesser Hinggan-Zhangguangcai Range in NE China. Data sources: The Sr-Nd-Hf isotopic data of arc magmas from the continental arcs (Kamchatka and Honshu) and oceanic arcs (Izu-Bonin-Mariana) in the western Pacific are collected from the database GEOROC (http://georoc.mpch-mainz.gwdg.de/georoc) and listed in the Data Set S4. Fields of zircon-free and zircon-bearing sedimentary rocks are from Bayon et al. (2009). Other data sources: mafic intrusions in the Lesser Hinggan-Zhangguangcai Range (Guo et al., 2015); depleted mantle in NE China (Guo et al., 2009; Miao et al., 2008); Terrigenous sediment represented by the compositions of average upper continental crust (UCC; James, 1981); and pelagic sediment from western Pacific (Cousens et al., 1994; J. A. Pearce et al., 1999; Woodhead, 1989).

diorites, four samples from the Kaishantun diorite have lower initial $^{87}Sr/^{86}Sr(i)$ (0.7043–0.7046) and higher $\varepsilon_{Nd}(t)$ (+4.8 to + 5.3) and $\varepsilon_{Hf}(t)$ values (+12.0 to +12.3). In general, the Early Jurassic mafic intrusive rocks show Sr-Nd-Hf isotopic compositions within the ranges of arc magmas in the western Pacific (Figure 7).

Compared to the synchronous mafic intrusions in the LHZR—the northern part of the subduction zone, the Yanbian diorites have similar Nd and Hf isotopic compositions but clearly lower radiogenic Sr isotopes (Figure 7; Guo et al., 2015). Two variation trends can be identified: The Yanbian mafic rocks define a Sr-Nd isotopic array toward the terrigenous sediments, whereas the LHZR mafic counterparts show another Sr-Nd isotopic array toward pelagic sediments (Figure 7a). However, the mafic rocks from both the Yanbian area and the LHZR lie along the igneous rock array between the oceanic and continental arc magmas in the Nd-Hf isotopic diagram (Figure 7b; Bayon et al., 2009).

5. Discussion

The Early Jurassic Yanbian mafic rocks are characterized by calc-alkaline affinities, LREE and LILE enrichments, and HFSE depletion (e.g., Nb and Ta), which are typically observed in modern subduction-related mafic magmas (Elburg et al., 2002; Harry & Green, 1999). The geochemical signatures of the Yanbian mafic rocks could reflect a combination of shallow-level, crustal-chamber processes involving magmatic differentiation and crustal assimilation or could be explained by deeper, source-related process. In the following, we will first discuss the roles of magmatic differentiation and source enrichment in the generation of these mafic rocks and then reconstruct the architecture of Paleo-Pacific subduction zone in NE China.

5.1. Magmatic Differentiation

5.1.1. Crustal Contamination or AFC Processes

The Early Jurassic mafic rocks in the Yanbian area show large Sr-Nd-Hf isotopic variations over wide compositional ranges. However, each individual pluton shows quite homogeneous Sr-Nd-Hf isotopic compositions. These features may be attributed to variable proportions of crustal input into the mantle source or to crustal contamination and/or assimilation coupled with fractional crystallization (AFC) during magma ascent. Both processes may modify the chemical and isotopic compositions of the evolved melt. Thus, evaluating the effects of crustal or source contamination is critical to assess the nature of mantle source (original or modified) for the Yanbian mafic intrusions. In the following text, we will discuss the role of crustal contamination or AFC processes in the petrogenesis of individual intrusion.

1. The Yanbian mafic rocks generally show a positive correlation between $^{87}Sr/^{86}Sr(i)$ ratio and Sr concentration (Figure 8a), which is quite different from that is expected for crustal contamination since the upper continental crust generally has a lower Sr concentration but higher $^{87}Sr/^{86}Sr$ ratio than all the Yanbian mafic rocks (Rudnick & Gao, 2003; Wedepohl, 1995).
2. The effect of source or crustal contamination can be distinguished by using Sr-O isotope correlation (James, 1981), that is, source contamination causes a small increase in $\delta^{18}O_{VSMOW}$ and a significant increase in $^{87}Sr/^{86}Sr$, whereas crustal contamination will lead to a faster increase in $\delta^{18}O_{VSMOW}$ than $^{87}Sr/^{86}Sr$. According to Valley et al. (2005), we calculated the whole-rock $\delta^{18}O_{VSMOW}$ by using the equation:

$$\Delta^{18}O(\text{zircon}-\text{rock}) = \delta^{18}O\ (\text{zircon}) - \delta^{18}O\ (\text{rock}) \approx -0.0612\ (\text{wt.\%SiO}_2) + 2.5.$$

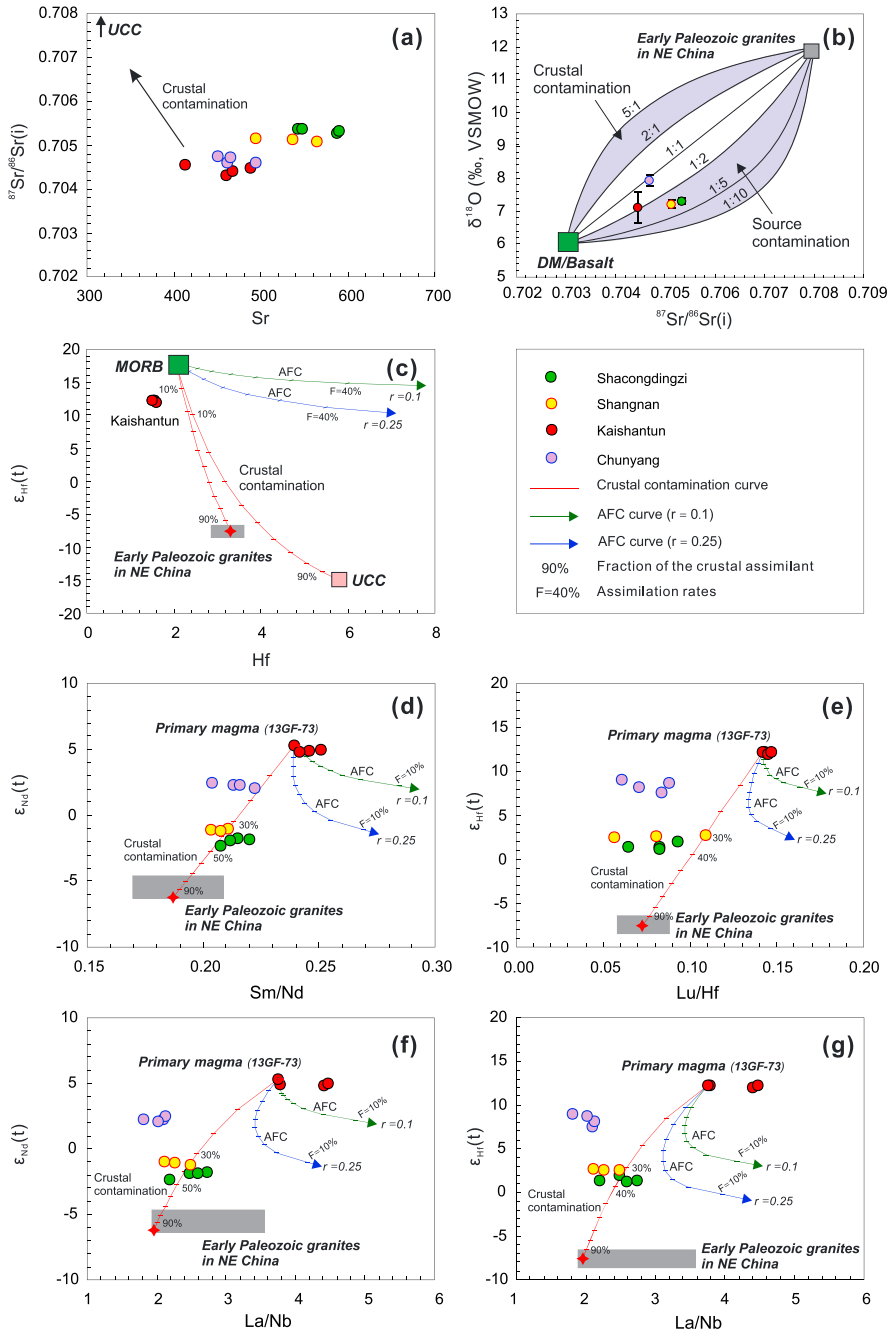

Figure 8. (a) $^{87}Sr/^{86}Sr(i)$ versus Sr, (b) whole-rock $\delta^{18}O_{VSMOW}$ versus $^{87}Sr/^{86}Sr(i)$ (James, 1981), (c) $\varepsilon_{Hf}(t)$ versus Hf, (d) $\varepsilon_{Hf}(t)$ versus Sm/Nd, (e) $\varepsilon_{Hf}(t)$ versus Lu/Hf, (f) $\varepsilon_{Nd}(t)$ versus La/Nb, and (g) $\varepsilon_{Hf}(t)$ versus La/Nb plots for the Yanbian mafic intrusions. In (a), the Sr concentration and $^{87}Sr/^{86}Sr(i)$ for the upper continental crust (UCC) are according to Wedepohl (1995). In (b), the $\delta^{18}O_{VSMOW}$ and $^{87}Sr/^{86}Sr$ for depleted mantle (DM)/basalt are 6 and 0.703 (James, 1981), the $^{87}Sr/^{86}Sr$ for the Early Paleozoic granitic rocks in NE China is 0.708 (according to Shimoda et al., 1998, and Wu et al., 2003), and the whole-rock $\delta^{18}O_{VSMOW}$ is calculated according to the inherited zircons in this study. AFC modeling (Depaolo, 1981; Powell, 1984) and crustal contamination results are shown in (c) to (g). In the AFC modeling, *r* values (0.1 and 0.25) denote the assimilation rates (a ratio of the rate of assimilation to the rate of fractional crystallization). Tick marks on the AFC modeling curves indicate the fraction of the residual magma (*F*). Tick marks on the crustal contamination modeling curves indicate the fraction of the crustal assimilant. All curves have tick marks at 10% increments. MORB has Hf = 2.05 (Sun & McDonough, 1989) and $\varepsilon_{Hf}(t) = +18$ (Guo et al., 2009, Miao et al., 2008), and average UCC has Hf = 5.8 ppm (Wedepohl, 1995) and $\varepsilon_{Hf}(t) = -15$ (Chauvel et al., 2014). The primary melt (13GF-73) has Lu = 0.22 ppm, Hf = 1.55 ppm, Sm = 2.61 ppm, Nd = 10.90 ppm, La = 7.32 ppm, Nb = 1.95 ppm, and $\varepsilon_{Nd}(t) = +5.3$ and $\varepsilon_{Hf}(t) = +12.3$. The assumed assimilant (Early Paleozoic granitic rocks in NE China) has Lu = 0.24 ppm, Hf = 3.30 ppm, Sm = 4.71 ppm, Nd = 25.13 ppm, La = 16.90 ppm, Nb = 8.62 ppm, $\varepsilon_{Nd}(t) = -6.2$ (according to Wu et al., 2003, and Z. W. Wang, Pei, et al., 2016), and $\varepsilon_{Hf}(t) = -8.4$ (according to $\varepsilon_{Hf}(t)$ of the early Paleozoic inherited zircons in this study). During AFC modeling, the bulk partition coefficients (K_D) for Lu, Hf, Sm, Nd, La, and Nb are 0.1, 0.2, 0.4, 0.5, 0.2, and 0.4, respectively. See detailed discussion in the text. MORB = mid-ocean ridge basalt; AFC = assimilation coupled with fractional crystallization.

We assume that the mantle/basalt end-member component has $^{87}Sr/^{86}Sr = 0.703$ and $\delta^{18}O_{VSMOW} = 6.0‰$ (James, 1981), and the crustal component has $^{87}Sr/^{86}Sr = 0.708$ (Wu et al., 2003) and $\delta^{18}O_{VSMOW} = 12‰$ (according to the $\delta^{18}O_{VSMOW}$ of the inherited Early Paleozoic zircons in this study). In the plot of $\delta^{18}O_{VSMOW}$ versus $^{87}Sr/^{86}Sr(i)$ diagram (Figure 8b), the Yanbian mafic rocks cluster along the convex-downward curves, indicating a source contamination rather than crustal contamination of a mantle-derived magma.

3. Among the four mafic intrusions, the Kaishantun diorites have the highest $\varepsilon_{Nd}(t)$ and $\varepsilon_{Hf}(t)$. Regardless of inherited Early Paleozoic zircons, a striking feature of these rocks is their lower Hf concentration and $\varepsilon_{Hf}(t)$ than those of average MORB (Figure 6c; S. S. Sun & McDonough, 1989; Workman & Hart, 2005). Since MORBs are high-degree melts from the convecting depleted mantle, they should have very low Hf contents and highly radiogenic Hf isotopic compositions. Given that the continental crust beneath the Yanbian area has high Hf concentration and unradiogenic Hf isotopic composition (Z. W. Wang, Pei, et al., 2016, and this study), it is unlikely that the Kaishantun diorites were formed through crustal contamination of a low-Hf and high-ε_{Hf} magma such as MORB. Similarly, these rocks can neither be produced by AFC processes of a MORB-type magma. Furthermore, crustal contamination and AFC modeling (Depaolo, 1981; Powell, 1984) was performed to evaluate the possible role of such processes in the generation of the Kaishantun diorites. We selected a MORB-like melt as the primary magma and the average composition of the early Paleozoic granitic rocks in NE China (~430 Ma; Z. W. Wang, Pei, et al., 2016; Wu et al., 2003) as the average continental crust to represent a felsic assimilant. With the assimilation rate (r) between 0.1 and 0.25, the Kaishantun diorites plot distant from the AFC modeling curves, indicating an insignificant role of AFC processes (Figure 8c). Moreover, the modeling results also suggest a minor role of contamination of the felsic assimilant or average upper continental crust in their generation (Figure 6c). Thus, a likely origin for the inherited zircons (e.g., 401–445 Ma) in the Kaishantun diorites may originate from the subducted terrigenous sediments, since zircon has the capacity to survive under high-temperature and high-pressure conditions (Dai et al., 2011, 2017; Valley, 2003).
4. The Shacongdingzi, Shangnan, and Chunyang plutons show lower Sm/Nd, Lu/Hf, La/Nb, $\varepsilon_{Nd}(t)$, and $\varepsilon_{Hf}(t)$ than those of the Kaishantun pluton (Figures 8d–8g). These elemental and isotopic variations among the four mafic intrusions indicate that these three plutons may be generated by crustal contamination or AFC of the Kaishantun mafic magma. Thus, crustal contamination and AFC modeling was also performed to evaluate the possible role of such processes in the generation of these three dioritic intrusions. Here we select the sample 13GF-73 from the Kaishantun intrusion that has the highest MgO, $\varepsilon_{Nd}(t)$, and $\varepsilon_{Hf}(t)$ values to be the candidate for the primary magma and the average composition of the early Paleozoic granitic rocks in NE China (~430 Ma; Z. W. Wang, Pei, et al., 2016; Wu et al., 2003) as the average continental crust to represent a felsic assimilant. With the assimilation rate (r) between 0.1 and 0.25, the samples from the other three mafic intrusions plot distant from the modeling curves, indicating an insignificant role of AFC processes in their formation (Figures 8d–8g). Furthermore, crustal contamination modeling results suggest addition of 30–50% of continental crustal components into the parental magma-like sample 13GF-73 to produce the geochemical and isotopic compositions of the three mafic intrusions (Figures 8d–8g). However, addition of such a large volume of continental crustal component could not be reequilibrated for the heat budget (Fan et al., 2004). Thus, the modeling results suggest that the other three mafic intrusions cannot be formed through crustal assimilation of the Kaishantun dioritic magma. The absence of crustal xenoliths in these three mafic intrusions also suggests a negligible role of bulk contamination by the wall rocks during magmatic evolution.

Summarizing, it is reasonable to conclude that the role of crustal contamination or AFC processes was minor in the petrogenesis of the early Jurassic mafic intrusions.

5.1.2. Fractional Crystallization

Although likely of mantle origin, most of the Yanbian diorite samples have low MgO or Mg# and compatible element concentrations (e.g., Cr, Ni, and Co) relative to contemporaneous ultramafic-mafic rocks in NE China (Figure S3; Guo et al., 2015; Yu et al., 2012). Hence, the Yanbian diorites cannot represent primary mantle-derived magmas, and fractional crystallization could explain some of the systematic geochemical variations. Fractional crystallization can lead to systematic geochemical variations. Both MgO and Fe_2O_3 correlate negatively with SiO_2, suggesting a role of fractionation of ferromagnesian minerals (e.g., hornblende and clinopyroxene; Figure S3). Nickel and Cr are well correlated in most of the Yanbian diorites,

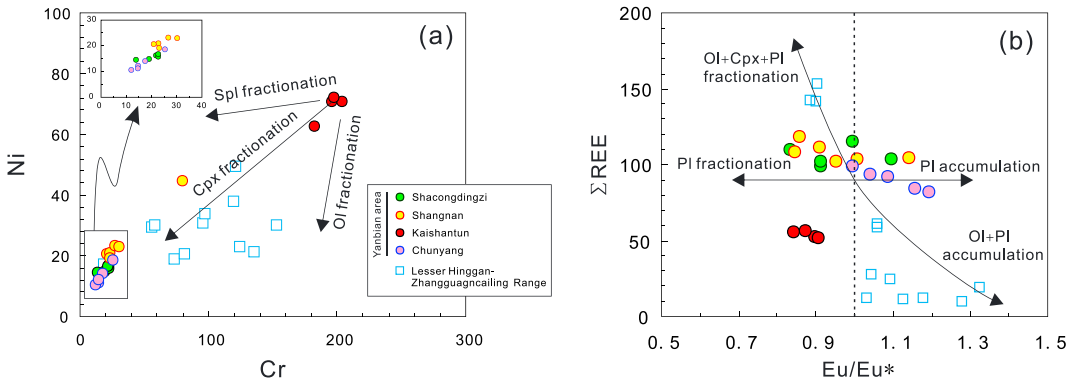

Figure 9. Plots of (a) Ni versus Cr (Pfänder et al., 2002) and (b) Total REE versus Eu/Eu* diagrams for the Yanbian mafic intrusions, showing the roles of fractionation and/or accumulation of clinopyroxene and plagioclase in the magma evolution. Data for mafic intrusive rocks from the Lesser Hinggan-Zhangguangcai Range are from Yu et al. (2012). Sp = spinel; Cpx = clinopyroxene; Pl = plagioclase; Ol = olivine; REE = Rare Earth Elements.

indicating either substantial clinopyroxene fractionation and/or combined olivine and spinel fractionation (Figure 9a; Pfänder et al., 2002). Likewise, the positive correlation between Al_2O_3 and SiO_2 but negative correlation between CaO and SiO_2 indicate clinopyroxene and minor plagioclase fractionation (Figure S3). Most samples have Eu/Eu^* marginally higher than 1.0 and also show weak (moderately in the case of the Kaishantun diorite) positive Sr and Eu anomalies, additionally indicating a role of minor plagioclase accumulation (Figures 6 and 9b). Thus, a fractional assemblage of olivine/spinel + clinopyroxene + hornblende + plagioclase may be responsible for the elemental variations observed within these mafic rocks in the Yanbian area.

5.2. The Role of Subducted Sediments in the Mantle Sources

5.2.1. Enrichment Mechanisms in the Mantle Sources: Fluid or Melt?

Numerous studies on the arc magmatism have demonstrated that the subarc mantle is usually modified by the subducting slab and the overlying sediments (e.g., Churikova et al., 2001; Hawkesworth et al., 1993; Marini et al., 2005). The mantle wedge above a subducted slab can be enriched by the addition of (1) aqueous fluid derived from dehydration of the subducting slab and/or (2) silicate melt derived from melting of the subducted sediments (e.g., Churikova et al., 2001; Elburg et al., 2002; Woodhead et al., 2001). As a result of the different geochemical behaviors in fluids and melts, some elements can be used to decipher the contribution of fluids and melts to a depleted mantle wedge. For instance, aqueous fluid usually has high concentrations of fluid-mobile trace elements such as LILE (e.g., K, Rb, Sr, and Ba) and Pb but low concentrations of LREE, Th, and HFSE (e.g., Zr, Hf, Nb, and Ta) from the subducting slab to the mantle wedge. In contrast, the silicate melt of the subducted sediments contains high contents of Th, LREE, and LILE. Thus, subduction-related magmas derived from fluid-metasomatized mantle sources have higher LILE/LREE, LILE/HFSE, and LILE/Th ratios than those derived from melt-modified mantle source regions. Ratios of fluid-mobile trace elements to fluid-immobile trace elements may effectively identify the role of fluid from melt of the subducted sediments in the mantle source (Woodhead et al., 2001).

Here we use the Ba/La, Rb/Nb, and Th/Yb ratios to constrain the respective role of slab fluids and melts in the petrogenesis of the Early Jurassic mafic intrusions across the arc magmatic belt (Figures 10a and 10b). For the southern Yanbian mafic rocks, the Shacongdingzi, Shangnan, and Chunyang intrusions display low Ba/La and Rb/Nb and high Th/Yb ratios, indicating a predominant role of sediment melt in their mantle sources. The Kaishantun diorites, which have the highest Ba/La and Rb/Nb ratios, show a dominant contribution from a slab-fluid component. The northern LHZR mafic rocks display a small variability in Ba/La and Rb/Nb accompanied by a large variability in Th/Yb (Figures 10a and 10b), suggesting an increasing contribution of sediment melt to their source. Consequently, except for the Kaishantun diorites which were predominantly derived from a fluid-enriched mantle source, the other mafic rocks in the Yanbian area and the LHZR region were derived from the mantle sources enriched by the predominant sediment melts.

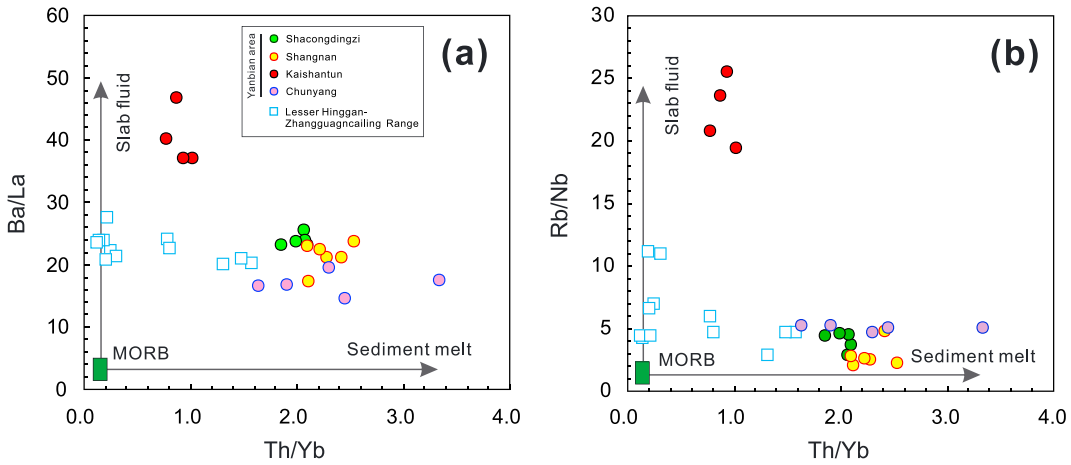

Figure 10. (a) Ba/La versus Th/Yb and (b) Rb/Nb versus Th/Yb diagrams showing the possible enriched components in the mantle source of the Early Jurassic mafic rocks from Yanbian area and Lesser Hinggan-Zhangguangcai Range in NE China (Yu et al., 2012). MORB = mid-ocean ridge basalt.

5.2.2. Terrigenous Sediments in the Mantle Source of Yanbian Mafic Rocks

The Early Jurassic Yanbian mafic rocks are characterized by depletion of Nb and Ta (Figure 6). Generally, the Nb-Ta depletion in arc mafic magmas is attributed to an addition of LILE- and/or LREE-enriched and Nb-Ta-depleted slab-derived fluids and melts to the depleted mantle wedge (e.g., Baier et al., 2008; Handley et al., 2007; J. A. Pearce & Peate, 1995). Moreover, relative to MORBs, the Yanbian mafic rocks have less radiogenic Nd and Hf but more radiogenic Sr isotopic compositions and also have zircon $\delta^{18}O_{VSMOW}$ higher than normal mantle value (Figures 4b and 7), indicating the involvement of subducted sediments in their mantle source. The zircon Hf-O isotopic variations, which suggest a mixing trend between a depleted mantle and a sediment component, can best be explained by the involvement of terrigenous and pelagic sediments, respectively (Figure 4c).

On the other hand, the inheritance of the Early Paleozoic zircons leads to nonradiogenic Hf ($\varepsilon_{Hf}(t) = -8.4$ to -6.7) and $\delta^{18}O_{VSMOW}$ as high as 9.0‰ (Figures 4a and 4b). Since we have excluded significant crustal assimilation during the magmatic evolution, the nonradiogenic Hf and elevated O isotopic compositions of inherited zircons further confirm their derivation from the Paleozoic terrane in the Yanbian area (Z. W. Wang, Pei, et al., 2016; Wu et al., 2003; Zhou & Wilde, 2013). In addition, their Sr-Nd isotopic array toward terrigenous sediment indicates the involvement of terrigenous sediments in their origin (Figure 7a). Such inherited zircons have also been reported in the deep-seated magma elsewhere in the world (e.g., Sulu-Dabie orogeny) since zircon has the capacity to survive under high-temperature and high-pressure conditions (Dai et al., 2011, 2017). Furthermore, the sedimentary component of the Kaishantun ophiolitic mélange in the Yanbian area consists predominantly of sandstone, conglomerate, and mudstone (Shao & Tang, 1995), indicating a terrigenous origin of the subducted sediments. Finally, the mafic intrusions are calc-alkaline in character and were formed in a continental arc (Figure 5), also implying the predominant role of subducted terrigenous sediments. Accordingly, the mantle source for the Early Jurassic Yanbian mafic intrusions was mainly enriched by subducted terrigenous sediments.

5.2.3. Compositionally Distinct Sediment Input Across the Subduction Zone

In NE China, besides the early Jurassic Yanbian mafic intrusions in the south, contemporaneous mafic rocks are also distributed in the LHZR—the northern segment of the subduction zone (Guo et al., 2015; Yu et al., 2012). These mafic rocks show tholeiitic affinities (Figures 5a and 5b). Compared to the Yanbian mafic intrusions, they have higher Sr isotope ratios at a given $\varepsilon_{Nd}(t)$ (Figure 7a). Regardless of the high $^{87}Sr/^{86}Sr(i)$, geochemical features such as low K, Rb, and Th argue against an important role of continental crustal contamination or assimilation in their petrogenesis. Instead, the previous studies considered that their mantle source was modified by subducted sediments (Guo et al., 2015; Yu et al., 2012). However, the provenance (pelagic vs. terrigenous) of the subducted sediments remains unclear. In the following, we will combine the geochemical proxy and geological records to address this issue.

Because of the "zircon effect" during transportation, the pelagic and terrigenous sediments have distinct chemical compositions, that is, pelagic sediments have lower Hf/Nd and higher Lu/Hf ratios and develop more radiogenic Hf with time than those of terrigenous sediments (Bayon et al., 2009; David et al., 2001; Marini et al., 2005; Plank & Langmuir, 1998; Vervoort et al., 1999, 2011). Also, the continent-derived detritus generally has much higher Th concentrations than the pelagic detritus and has higher Th/REE ratios (Plank & Langmuir, 1998). In NE China, however, the Yanbian mafic rocks display Nd-Hf isotopic array along the arc igneous rock array, which is similar to those of the LHZR mafic rocks (Figure 7b). As discussed above, the subducted sediments added into the mantle source of the Yanbian mafic rocks were mainly derived from the Early Paleozoic (~430 Ma) granitic rocks or terranes in NE China. The time for transportation and deposition of the source protoliths is too short to produce the Nd-Hf isotopic decoupling as observed in the Himalaya sandstones (Richards et al., 2005). Although the Yanbian mafic rocks were likely derived from the mantle wedge enriched by subducted terrigenous sediments, they plot within the Hf-Nd isotopic array of arc igneous rocks (Figure 7b). Actually, the mafic rocks from the modern continental arcs (e.g., Kamchatka and Honshu arcs) and oceanic arcs (e.g., Izu-Bonin and Mariana arcs) in the western Pacific also show Nd-Hf correlations along the terrestrial array without Nd-Hf decoupling (Figure 7b).

Thus, Th/REE and Hf/REE ratios of the mafic rocks can be applied to trace the provenance of subducted sediments. In fact, Lu/Hf, Th/La, and Th/Yb ratios have been widely used to track the contribution of sediments to enrichment processes of subarc mantle (Plank, 2005; Plank & Langmuir, 1998; Woodhead et al., 2001). In NE China, except for the Kaishantun diorites which were derived from a mantle source modified by a fluid component (Figure 10), the mafic intrusions show similar Ba/La and Rb/Nb ratios that indicate similar degrees of fluid metasomatism in their mantle sources. For the purpose of comparison, we select those early Jurassic mafic intrusions with similar Ba/La and Rb/Nb ratios to further distinguish the sediment input. In Lu/Hf versus Th/La and Lu/Hf versus Th/Yb plots, the mafic rocks from the northern LHZR clearly have higher Lu/Hf and lower Th/La and Th/Yb ratios than those from southern Yanbian area (Figures 11a and 11b), indicating that the mantle source of the Yanbian mafic rocks was predominantly enriched by terrigenous sediments, whereas the mantle source for the LHZR mafic intrusions was likely metasomatized by a component composed mainly of pelagic sediments. On the other hand, in the northern segment of the subduction zone, deep-sea oceanic radiolarian silicalite, cherts, and oozes of pelagic origin are well developed in the subduction-accretionary complexes such as the Heilongjiang Complex, Raohe Complex, and the accretionary wedge in the southern Sikhote-Alin orogenic belt of the Russian Far East (Cheng et al., 2006; K. Liu, Zhang, Wilde, Liu, et al., 2017; Zhou et al., 2009, 2014). The sedimentary records also indicate the important contribution of subducted pelagic sediments to the enrichment process of subarc mantle beneath the northern segment of NE China.

In summary, the geochemical difference between the southern Yanbian and northern LHZR mafic intrusions can be interpreted as a result of input of compositionally distinct subducted sediments into the mantle source through the arc magmatic belt. Such geochemical variations of arc basalts can also be found in modern subduction zones, for example, the Kamchatka-Honshu-Izu-Bonin-Mariana arc systems in the western Pacific (e.g., Bergal-Kuvikas et al., 2017; Elliott et al., 1997; Freymuth et al., 2016; Hoang et al., 2013). The continental arc mafic rocks (e.g., in the Kamchatka and Honshu arcs) derived from a mantle wedge enriched by addition of predominantly subducted terrigenous sediments also have higher Th/La and Th/Yb and lower Lu/Hf ratios than those oceanic arc basalts (e.g., in the Izu-Bonin-Mariana arcs), which originate from a mantle source metasomatized by subducted pelagic sediments (Figures 11c and 11d).

5.2.4. Subarc Mantle Enrichment by Subducted Sediments

Previous studies have demonstrated that terrigenous sediments usually have higher Hf/Sm but lower Ba/Nb ratios than those of pelagic sediments (e.g., Richards et al., 2005), we thus use the correlations between these two geochemical proxies and $\varepsilon_{Nd}(t)$ and $\varepsilon_{Hf}(t)$ to further evaluate the contribution of the two types of sediments to the subarc mantle enrichment across the belt (Figure 12). In NE China, the possible provenance for the terrigenous sediments includes the Khanka, Jiamusi, and Hinggan Massifs and the suturing orogenic belts between these terrains. According to Zhou and Wilde (2013), these massifs are composed mainly of Pan-African metaigneous protoliths and metasedimentary granulites, intruded by Early Paleozoic granitoids. Both the metasedimentary granulites and granitic rocks have highly evolved isotopic compositions (Wu et al., 2000, 2003). For our modeling, we use the composition of the upper continental crust to approximate the terrigenous sediment component because of the only limited geochemical data exist for these

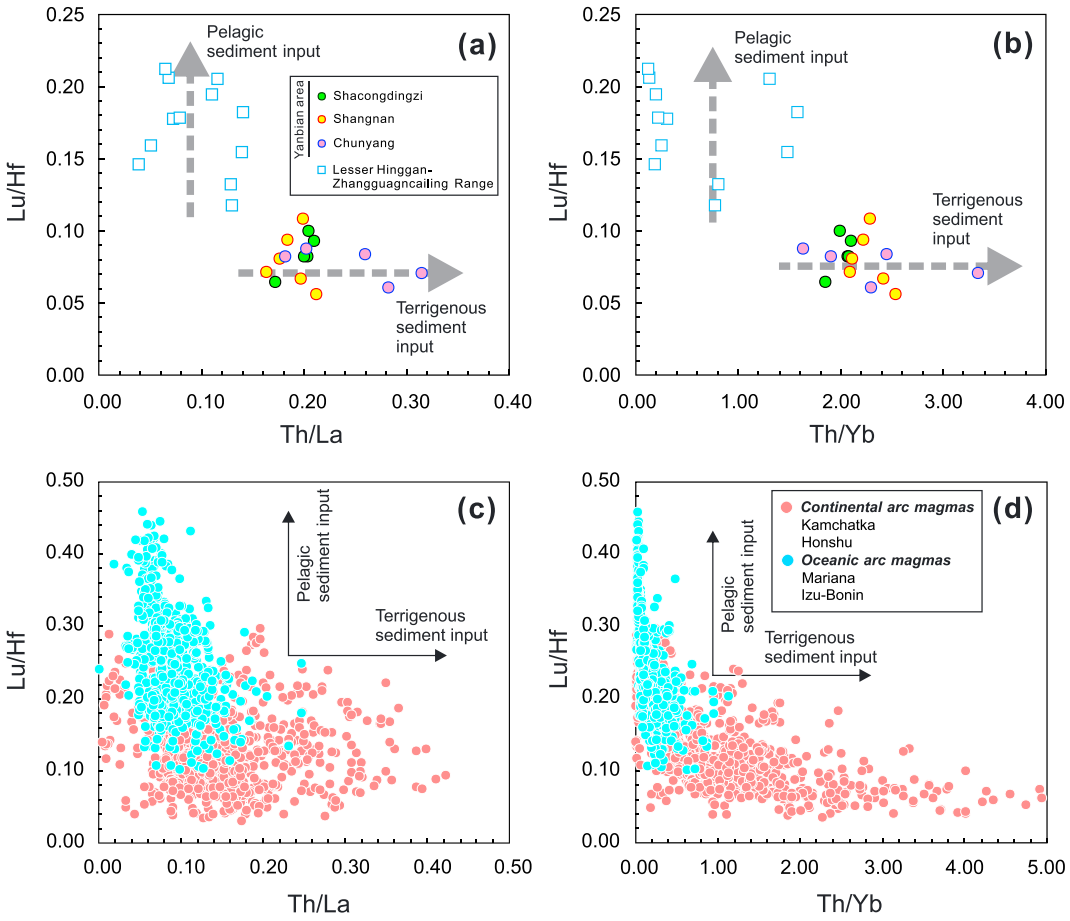

Figure 11. (a) Lu/Hf versus Th/La and (b) Lu/Hf versus Th/Yb diagrams showing the possible subducted sediments in the mantle source of the Early Jurassic mafic rocks from Yanbian area and Lesser Hinggan-Zhangguangcai Range in NE China (Yu et al., 2012). The directions of arrow indicate that of the Early Jurassic mafic rocks from Yanbian area and Lesser Hinggan-Zhangguangcai Range in NE China were mainly modified by terrigenous sediments and pelagic sediments, respectively. (c) Lu/Hf versus Th/La and (d) Lu/Hf versus Th/Yb plots showing a comparison of mafic rocks between the modern continental arcs (Kamchatka and Honshu) and oceanic arcs (Izu-Bonin-Mariana) in the western Pacific. Data sources for the Kamchatka, Honshu, and Izu-Bonin-Mariana arcs are collected from the database GEOROC (http://georoc.mpch-mainz.gwdg.de/georoc) and listed in Data Set S4.

Paleozoic terrains. Also, we select the deep-sea siliceous rocks from the western Pacific to represent the subducted pelagic sediment component (e.g., Cousens et al., 1994; J. A. Pearce et al., 1999; Woodhead, 1989). At the same time, we assume a depleted mantle as the other end-member candidate. Trace element and isotopic modeling results show that the compositional range of the Yanbian mafic intrusive rocks is consistent with derivation from a depleted mantle wedge metasomatized by a variable addition (2–10%) of terrigenous sediments (Figure 12). Additionally, the mafic rocks in the LHZR were plausibly formed by melting of a depleted mantle source enriched by addition of 3–10% melt of pelagic sediment (Figure 12). Again, the Kaishantun diorites have compositions different from the other mafic intrusions in the Yanbian area and were derived from a mantle source predominantly enriched by sediment fluids (Figures 12c and 12d).

In summary, we identify two distinct subducted sediment components involved in the enriched mantle sources beneath NE China. To the south, the mantle wedge beneath what is now the Yanbian area was mainly contaminated by addition of subducted terrigenous sediments, and enrichment was both fluid- and melt-induced. In the north, the mantle wedge beneath what is now the LHZR was largely enriched by subducted pelagic sediments.

5.3. Geological Implications

5.3.1. Geological Records of the Paleo-Pacific Oceanic Subduction in NE China

The Phanerozoic tectonic evolution of NE China has been mainly controlled by the Paleo-Asian Oceanic subduction and the subsequent tectonic superimposition through the Paleo-Pacific slab subduction (e.g.,

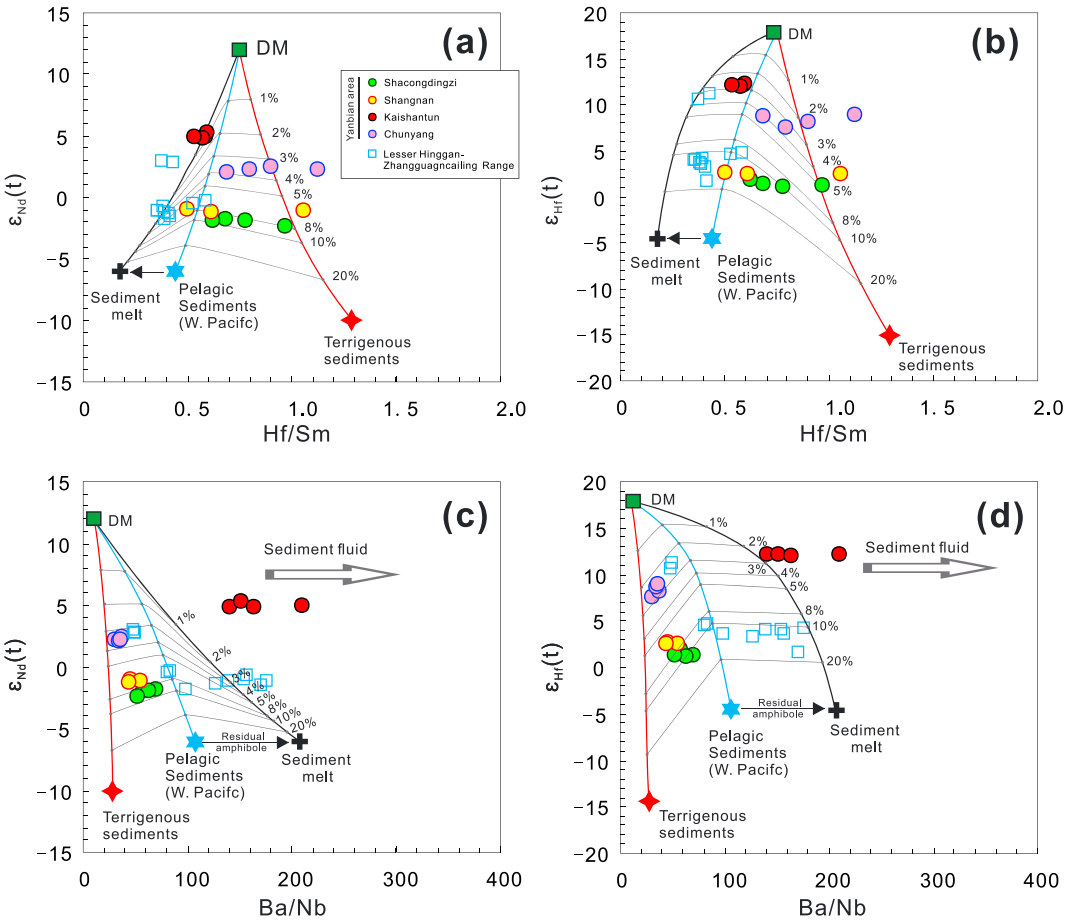

Figure 12. (a) $\varepsilon_{Nd}(t)$ versus Hf/Sm, (b) $\varepsilon_{Hf}(t)$ versus Hf/Sm, (c) $\varepsilon_{Nd}(t)$ versus Ba/Nb, and (d) $\varepsilon_{Hf}(t)$ versus Ba/Nb diagrams of Early Jurassic mafic rocks, showing the role of subducted sediments in the mantle enrichment beneath the Yanbian area and Lesser Hinggan-Zhangguangcai Range in NE China. Trace element concentrations and Nd and Hf isotopic data of the mafic rocks from Lesser Hinggan-Zhangguangcai Range are from Yu et al. (2012) and Guo et al. (2015), respectively. Neodymium and Hf concentrations and Nd-Hf isotopic compositions of the end-member components in (c)–(f) are the same as in Figure 8. Other parameters used in the modelling are (1) DM has Ba = 3 ppm, Nb = 0.3 ppm, Hf = 0.3 ppm, Nd = 1.2 ppm, Sm = 0.4 ppm (based on Sun & McDonough, 1989), $\varepsilon_{Nd}(t) = +12$, and $\varepsilon_{Hf}(t) = +18$ (Guo et al., 2009, Miao et al., 2008); (2) pelagic sediment from the western Pacific (W. Pacific) has Ba = 1380 ppm, Nb = 13 ppm, Hf = 3.8 ppm, Nd = 36 ppm, Sm = 8.7 ppm (Cousens et al., 1994), $\varepsilon_{Nd}(t) = -6$ (Cousens et al., 1994), and $\varepsilon_{Hf}(t) = -4.5$ (J. A. Pearce et al., 1999; Woodhead, 1989); (3) terrigenous sediment (upper continental crust) has Ba = 668 ppm, Nb = 26 ppm, Hf = 5.8 ppm, Nd = 27 ppm, Sm = 4.5 ppm (Wedepohl, 1995), $\varepsilon_{Nd}(t) = -10$, and $\varepsilon_{Hf}(t) = -15$ (Chauvel et al., 2014). During partial melting of the pelagic sediments, the volume of sediment melt (F) is assumed to be 0.3, and the bulk partition coefficients (K_D) for Ba, Nb, Nd, Hf, and Sm are 0.1, 0.6, 0.05, 0.9, and 0.1, respectively. The numbers in percent shown on the tick marks of the curves denote the proportions of the subducted sediment being added into the mantle wedge. DM = depleted mantle.

Guo, 2016; Meng et al., 2011; Wu et al., 2000, 2011; W. L. Xu et al., 2013). However, it is a matter of active debate when subduction of the Paleo-Pacific Ocean beneath the Eurasian continent started. The proposed ages include Late Permian to Early Triassic (Ernst et al., 2007; M. D. Sun et al., 2015), Late Triassic (Zhou et al., 2014), and Early Jurassic (Guo et al., 2015; Wu et al., 2007; Yu et al., 2012).

The Early Jurassic Yanbian mafic intrusive rocks show elemental and isotopic signatures associated with the subduction of Paleo-Pacific slab. Recently, Yu et al. (2012) reported the N-S-trending belt of Early Jurassic (186–182 Ma) mafic intrusions belt along the LHZR. These mafic rocks were also attributed to melting of mantle wedge under a back-arc setting closely related to subduction of the Paleo-Pacific Ocean (Yu et al., 2012). In addition, Guo et al. (2015) proposed that the Early Jurassic (ca. 187 Ma) Tumen mafic intrusive complex was derived from a depleted mantle wedge metasomatized by hydrous sediment melt from the subducted Paleo-Pacific slab. Spatially, the Early Jurassic (188–173 Ma) Yanbian mafic intrusions represent the southern extent of the N-S-trending arc mafic magmatic belt.

The Heilongjiang Complex, which is located among the LHZR, Hinggan, and Jiamusi Massifs, has widely been regarded as a subduction-accretionary complex formed by westward subduction of the Paleo-Pacific

slab during 210–155 Ma (Ge et al., 2016; Wu et al., 2007; Zhou et al., 2009, 2014; Zhou & Wilde, 2013). These metamorphic complexes and the coeval I-type granitoids also constitute an N-S- trending metamorphic-magmatic belt, which coincides with the mafic magmatic belt (Figure 1c; F. Wang et al., 2015; Wu et al., 2011; W. L. Xu et al., 2013). The spatial association between arc magmatism and blueschist-facies metamorphism clearly indicates the westward subduction of the Paleo-Pacific Plate. Accordingly, the coexistence of the Early Jurassic mafic intrusions, metamorphic complexes, and the coeval I-type granitoids recorded the beginning of tectonic superimposition exerted by the Paleo-Pacific Oceanic subduction.

5.3.2. The Architecture of Paleo-Pacific Subduction Zone in NE China

NE China consists of a collage of several microcontinental massifs (e.g., Jiamusi, Khanka, Buleya, and Hinggan Massifs; Figure 1b). Although the Khanka, Jiamusi, and Buleya Massifs have widely been considered to have collided and amalgamated with the CAOB due to the Paleo-Pacific Oceanic subduction, the spatial distribution and timing of collision between them remains controversial (e.g., Chen et al., 2000; K. Liu, Zhang, Wilde, Zhou, et al., 2017; Z. W. Wang, Pei, et al., 2016; Wu et al., 2002, 2007; Zhou et al., 2014, 2009; Zhou & Wilde, 2013).

The mantle wedge in the south was predominantly metasomatized by addition of terrigenous sediments, which were probably from the Khanka, Jiamusi, and Buleya Massifs, as indicated by the presence of the inherited zircon with ages similar to rocks from those regions. This suggests that at least in the Early Jurassic, these Paleozoic terrains were still located in the southeastern CAOB. The sedimentary records and U- Pb ages of detrital zircons from the accretionary complexes in NE China and Far East of Russia also support such a hypothesis (K. Liu, Zhang, Wilde, Liu, et al., 2017; Z. W. Wang, Pei, et al., 2016; Zhou & Wilde, 2013). Thus, we develop a geodynamic model to link the petrogenesis of the Yanbian mafic intrusions with the Early Jurassic Paleo-Pacific Oceanic subduction. During the Early Jurassic, the Paleo-Pacific slab was subducted beneath the Paleozoic terrains (e.g., Khanka, Jiamusi, and Buleya Massifs). The terrigenous sediments that were eroded from these Paleozoic massifs, together with the oceanic lithosphere, were introduced into the mantle wedge. The fluids and melts released from the subducted slab (both the subducted sediments and altered oceanic crust) variably reacted with the depleted mantle wedge, forming compositionally distinct sources. Melting of the heterogeneous mantle wedge formed the Early Jurassic mafic intrusions in the Yanbian area and its adjacent regions.

The geochemical comparison of the Early Jurassic mafic intrusions between the southern and northern parts of the arc magmatic belt reveals an obvious difference in the provenance of the subducted sediments. This is supported by the tectonic discrimination diagrams (Figure 5). The Yanbian mafic intrusions are calc-alkaline and plot within the fields of continental arc, whereas the mafic intrusions from the LHZR are tholeiitic and fall into the fields of oceanic arc. This suggests that the mafic intrusions in the southern part of this arc magmatic belt were likely formed in a continental arc, whereas those in the northern part of the belt were probably generated in an oceanic arc. The Early Jurassic subduction zone in NE China might consist of both continental and oceanic arcs, analogous to the modern Kamchatka-Honshu-Izu- Bonin-Mariana arc systems in the western Pacific (Plank et al., 2007). Accordingly, we develop a cartoon to illustrate the tectonic evolution of the NE China since the Early Jurassic as follows (Figure 13):

1. The 190–170 Ma (Figures 13a and 13b). The Khanka-Jiamusi-Buleya Massif was located in the southern part of the subduction zone and separated from the CAOB by the Dunhua-Mishan Fault, which is one of the branches of the northern segment of Tan-Lu Fault (Figure 13a). The Paleo-Pacific Plate (i.e., the Izanagi Plate) was subducted beneath the Khanka-Jiamusi-Buleya Massif and formed an active continental margin (Figure 13b). In contrast, in the northern part of the subduction zone, the LHZR was separated from the CAOB by the Mudanjiang Ocean (Figure 13a). The Paleo-Pacific Plate subducted beneath the Mudanjiang Oceanic Plate and formed an oceanic arc (Figure 13b).
2. The 140–120 Ma (Figure 13c). With the oceanic ridge spreading and the strong displacement along the transform faults, the Paleo-Pacific Plate (Izanagi Plate) moved from a NW direction to a northward direction (Koppers et al., 2001; K. Liu, Zhang, Wilde, Liu, et al., 2017; Seton et al., 2012; W. D. Sun et al., 2007; J. W. Xu et al., 1987). Oblique subduction toward the East Asian continent occurred, leading to the large-scale strike-slipping movement of the Tan-Lu Fault System (J. W. Xu et al., 1987). The preexisting Khanka-Jiamusi-Buleya Massif was probably moved northward to the present-day position in response to the sinistral strike-slipping motion of the Dunhua-Mishan Fault (F. Wang, Xu, et al., 2016). At the

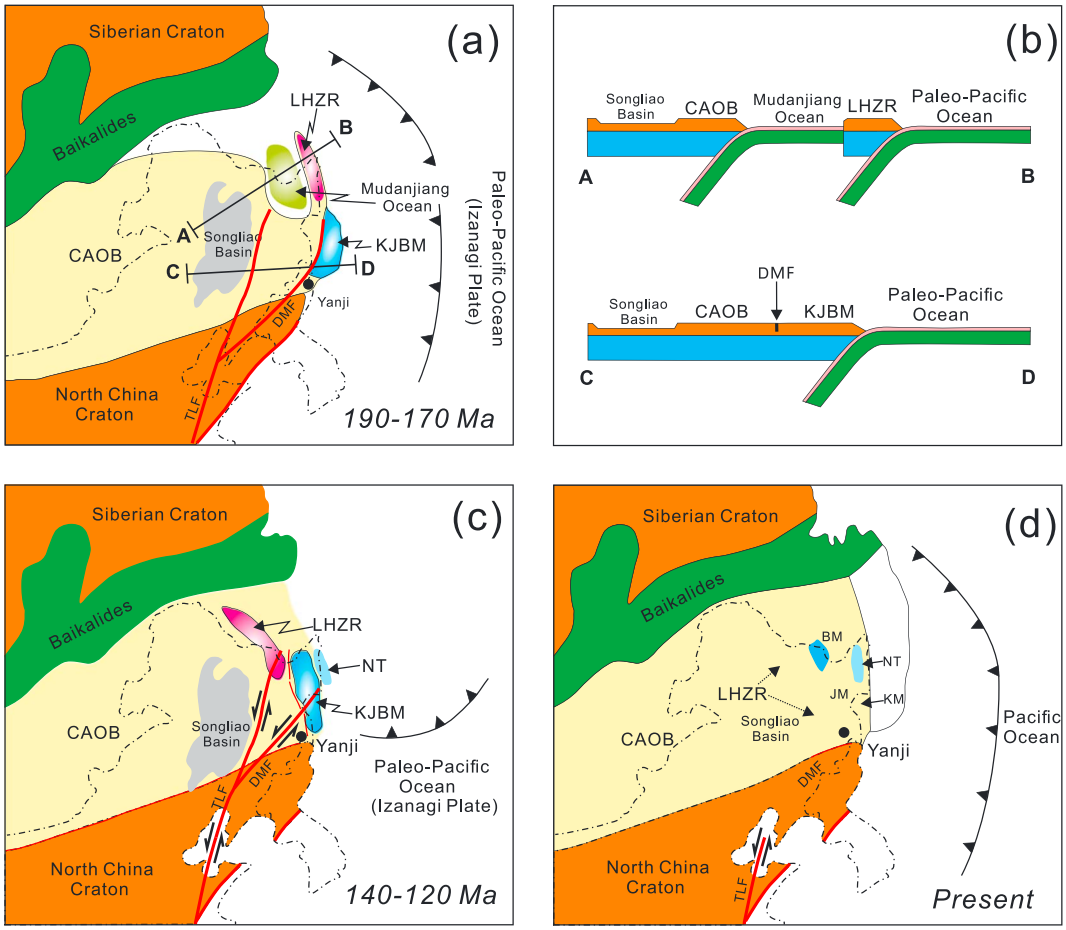

Figure 13. Reconstruction of the tectonic evolution of the NE China since the Early Jurassic. (a) Early Jurassic (190–170 Ma) subduction of the Paleo-Pacific Ocean (Izanagi Plate); (b) schematic cross sections showing the geodynamics of KJBM continental arc and LHZR island arc; (c) preexisted KJBM was moved to the present-day positions in response to the sinistral strike-slip movement of the DMF (140–120 Ma); and (d) present setting. See detailed discussion in the text. LHZR = Lesser Hinggan-Zhangguangcai Range; CAOB = Central Asian Orogenic Belt; KJBM = Khanka-Jiamusi-Buleya Massif; NT = Nadanhada Terrane; TLF = Tan-Lu Fault; DMF = Dunhua-Mishan Fault; BM = Buleya Massif; JM = Jiamusi Massif; KM = Khanka Massif.

same time, the Yanbian area moved eastward, and the LHZR retreated westward, forming the Late Mesozoic tectonic architecture of NE China.

3. The Present (Figure 13d). Due to rollback and retreat of the subducting Pacific slab and the subsequent opening of the Japan Sea and multiple-stage changes of moving direction of the Pacific Plate as well (Koppers et al., 2001; W. D. Sun et al., 2007; Y. Q. Zhang et al., 2003), the Khanka-Jiamusi-Buleya Massif and LHZR were divided into several micromassifs, and the present-day tectonic framework of NE China was ultimately formed.

6. Conclusions

Zircon U-Pb ages indicate that the Early Jurassic mafic intrusions in the Yanbian area were emplaced at 188–173 Ma, temporally consistent with the N-S-trending LHZR-Yanbian arc magmatic belt. The comprehensive geochemical results suggest the following conclusions:

1. The southern Yanbian mafic rocks are calc-alkaline and were derived from a mantle wedge variably enriched through predominant addition of subducted terrigenous sediments. In contrast, the mantle wedge in the northern part of the arc magmatic belt was mainly modified by the subducted pelagic sediments. Ratios of Hf and Th to REEs can be effective geochemical proxies to discriminate the provenance of subducted sediments.

2. The Early Jurassic subduction zone in NE China might consist of both continental and oceanic arcs, analogous to the modern Kamchatka-Honshu-Izu-Bonin-Mariana arc systems in the western Pacific.
3. The reconstructed architecture implies that the Mesozoic subduction of the Paleo-Pacific Ocean led to the sinistral strike-slipping movement of the Dunhua-Mishan Fault and displaced the Khanka-Jiamusi-Buleya Massif northward to the present position.

Acknowledgments
We sincerely thank Y. Liu, L. Qi, and Z. Y. Ren for whole-rock geochemistry and isotopic analyses and X.H. Li, J.H. Yang, and Y.H. Yang for in situ zircon U-Pb-Hf-O isotopic analyses. Constructive comments and suggestions from the Associate Editor John Lassiter, Christoph Beier, and an anonymous reviewer help to improve the quality of manuscript. Michael Walter is appreciated for his editorial handling. This work is financially supported by National Natural Science Foundation of China (41525006), the Strategic Priority Research Program (B) of Chinese Academy of Sciences (XDB18000000), and the National Key Basic Research Program of China (2013CB429804). Supplementary data related to this article are available in the supporting information. This is contribution No. IS-2659 from GIGCAS.

References

Aizawa, Y., Tatsumi, Y., & Yamada, H. (1999). Element transport by dehydration of subducted sediments: Implication for arc and ocean island magmatism. *Island Arc*, *8*(1), 38–46. https://doi.org/10.1046/j.1440-1738.1999.00217.x

Baertschi, P. (1976). Absolute ^{18}O content of standard mean ocean water. *Earth and Planetary Science Letters*, *31*(3), 341–344. https://doi.org/10.1016/0012-821X(76)90115-1

Baier, J., Audétat, A., & Keppler, H. (2008). The origin of the negative niobium tantalum anomaly in subduction zone magmas. *Earth and Planetary Science Letters*, *267*, 290–300. https://doi.org/10.1016/j.epsl.2007.11.032

Bayon, G., Burton, K., Soulet, G., Vigier, N., Dennielou, B., Etoubleau, J., et al. (2009). Hf and Nd isotopes in marine sediments: Constraints on global silicate weathering. *Earth and Planetary Science Letters*, *277*, 318–326. https://doi.org/10.1016/j.epsl.2008.10.028

Bergal-Kuvikas, O., Nakagawa, M., Kuritani, T., Muravyev, Y., Malik, N., Elimenko, E., et al. (2017). A petrological and geochemical study on time-series samples from Klyuchevskoy volcano, Kamchatka arc. *Contributions to Mineralogy and Petrology*, *172*, 35. https://doi.org/10.1007/s00410-017-1347-z

Bindeman, I. (2008). Oxygen isotopes in mantle and crustal magmas as revealed by single crystal analysis. *Reviews in Mineralogy and Geochemistry*, *69*, 445–478. https://doi.org/10.2138/rmg.2008.69.12

Black, L. P., Kamo, S. L., Allen, C. M., Aleinikoff, J. N., Davis, D. W., Korsch, R. J., & Foudoulis, C. (2003). TEMORA 1: A new zircon standard for Phanerozoic U-Pb geochronology. *Chemical Geology*, *200*(1-2), 155–170. https://doi.org/10.1016/S0009-2541(03)00165-7

Bouvier, A., Vervoort, J. D., & Patchett, P. J. (2008). The Lu–Hf and Sm–Nd isotopic composition of CHUR: Constraints from unequilibrated chondrites and implications for the bulk composition of terrestrial planets. *Earth and Planetary Science Letters*, *273*, 48–57. https://doi.org/10.1016/j.epsl.2008.06.010

Bureau of Geology and Mineral Resources of Jilin Province (BGMRJL) (1989). *Regional geology of Jilin Province* (in Chinese with English summary) (pp. 1–698). Beijing: Geological Press.

Cao, W. R., Lee, C. T. A., & Lackey, J. S. (2017). Episodic nature of continental arc activity since 750 Ma: A global compilation. *Earth and Planetary Science Letters*, *461*, 85–95. https://doi.org/10.1016/j.epsl.2016.12.044

Chauvel, C., Garçon, M., Bureau, S., Besnault, A., Jahn, B. M., & Ding, Z. L. (2014). Constraints from loess on the Hf-Nd isotopic composition of the upper continental crust. *Earth and Planetary Science Letters*, *388*, 48–58. https://doi.org/10.1016/j.epsl.2013.11.045

Chauvel, C., Lewin, E., Carpentier, M., Arndt, N. T., & Marini, J. C. (2008). Role of recycled oceanic basalt and sediment in generating the Hf-Nd mantle array. *Nature Geoscience*, *1*, 64–67. https://doi.org/10.1038/ngeo.2007.51

Chauvel, C., Marini, J. C., Plank, T., & Ludden, J. N. (2009). Hf-Nd input flux in the Izu-Mariana subduction zone and recycling of subducted material in the mantle. *Geochemistry, Geophysics, Geosystems*, *10*, Q01001. https://doi.org/10.1029/2008GC002101

Chen, B., Jahn, B. M., Wilde, S., & Xu, B. (2000). Two contrasting Paleozoic magmatic belts in northern Inner Mongolia, China: Petrogenesis and tectonic implications. *Tectonophysics*, *328*(1-2), 157–182. https://doi.org/10.1016/S0040-1951(00)00182-7

Cheng, R. Y., Wu, F. Y., Ge, W. C., Sun, D. Y., Liu, X. M., & Yang, J. H. (2006). Emplacement age of the Raohe Complex in eastern Heilongjiang Province and the tectonic evolution of the eastern part of Northeastern China (in Chinese with English summary). *Acta Petrologica Sinica*, *22*, 353–376.

Churikova, T., Dorendorf, F., & Wörner, G. (2001). Sources and fluids in the mantle wedge below Kamchatka, evidence from across-arc geochemical variation. *Journal of Petrology*, *42*(8), 1567–1593. https://doi.org/10.1093/petrology/42.8.1567

Clayton, R. N., Rex, R. W., Syers, J. K., & Jackson, M. L. (1972). Oxygen isotope abundance in quartz from Pacific pelagic sediments. *Journal of Geophysical Research*, *77*(21), 3907–3915. https://doi.org/10.1029/JC077i021p03907

Cousens, B. L., Allan, J. F., & Gorton, M. P. (1994). Subduction-modified pelagic sediments as the enriched component in back-arc basalts from the Japan Sea: Ocean Drilling Program Sites 797 and 794. *Contributions to Mineralogy and Petrology*, *117*(4), 421–434. https://doi.org/10.1007/BF00307275

Dai, L. Q., Zhao, Z. F., Zheng, Y. F., Li, Q. L., Yang, Y. H., & Dai, M. N. (2011). Zircon Hf–O isotope evidence for crust–mantle interaction during continental deep subduction. *Earth and Planetary Science Letters*, *308*, 229–244. https://doi.org/10.1016/j.epsl.2011.06.001

Dai, L. Q., Zheng, F., Zhao, Z. F., & Zheng, Y. F. (2017). Recycling of Paleotethyan oceanic crust: Geochemical record from postcollisional mafic igneous rocks in the Tongbai-Hong'an orogens. *Geological Society of America Bulletin*, *129*, 179–192. https://doi.org/10.1130/B31461.1

David, K., Frank, M., O'Nions, R. K., Belshaw, N. S., & Arden, J. W. (2001). The Hf isotope composition of global seawater and the evolution of the Hf isotopes in the deep Pacific Ocean from Fe-Mn crusts. *Chemical Geology*, *178*(1-4), 23–42. https://doi.org/10.1016/S0009-2541(00)00427-7

Depaolo, D. J. (1981). Trace element and isotopic effects of combined wallrock assimilation and fractional crystallization. *Earth and Planetary Science Letters*, *53*(2), 189–202. https://doi.org/10.1016/0012-821X(81)90153-9

Eiler, J. M. (2001). Oxygen isotope variations of basaltic lavas and upper and upper mantle rocks. *Reviews in Mineralogy and Geochemistry*, *43*(1), 319–364. https://doi.org/10.2138/gsrmg.43.1.319

Elburg, M. A., Bergen, M. A., Hoogewerff, J., Foden, J., Vroon, P., Zulkarnain, I., & Nasution, A. (2002). Geochemical trends across an arc-continent collision zone: Magma sources and slab-wedge transfer processes below the Pantar Strait volcanoes, Indonesia. *Geochimica et Cosmochimica Acta*, *66*(15), 2771–2789. https://doi.org/10.1016/S0016-7037(02)00868-2

Elliott, T. R., Plank, T., Zindler, A., White, W., & Bourdon, B. (1997). Element transport from slab to volcanic front at the Mariana arc. *Journal of Geophysical Research*, *102*(B7), 14,991–15,019. https://doi.org/10.1029/97JB00788

Ernst, W. G., Tsujimori, T., Zhang, R., & Liou, J. G. (2007). Permo-Triassic collision, subduction-zone metamorphism, and tectonic exhumation along the East Asian continental margin. *Annual Review of Earth and Planetary Sciences*, *35*, 73–110. https://doi.org/10.1146/annurev.earth.35.031306.140146

Fan, W. M., Guo, F., Wang, Y. J., & Zhang, M. (2004). Late Mesozoic volcanism in the northern Huaiyang tectono-magmatic belt, central China: Partial melts from a lithospheric mantle with subducted continental crust relicts beneath the Dabie orogen? *Chemical Geology*, *209*, 27–48. https://doi.org/10.1016/j.chemgeo.2004.04.020

Freymuth, H., Ivkoa, B., Gill, J. B., Tamura, Y., & Elliott, T. (2016). Thorium isotope evidence for melting of the mafic oceanic crust beneath the Izu arc. *Geochimica et Cosmochimica Acta*, *186*, 49–70. https://doi.org/10.1016/j.gca.2016.04.034

Gao, S., Liu, X. M., Yuan, H. L., Hattendorf, B., Gunther, D., Chen, L., & Hu, S. H. (2002). Determination of forty two major and trace elements in USGS and NIST SRM glasses by laser ablation-inductively coupled plasma-mass spectrometry. *Geostandards Newsletter-The Journal of Geostandards and Geoanalysis*, *26*(2), 181–196. https://doi.org/10.1111/j.1751-908X.2002.tb00886.x

Ge, M. H., Zhang, J. J., Liu, K., Ling, Y. Y., Wang, M., & Wang, J. M. (2016). Geochemistry and geochronology of the blueschist in the Heilongjiang Complex and its implications in the late Paleozoic tectonics of eastern NE China. *Lithos*, *261*, 232–249. https://doi.org/10.1016/j.lithos.2015.11.019

Guo, F. (2016). Geological records of the Pacific Plate subduction in the northeast Asian continental margin: An overview (in Chinese with English abstract). *Bulletin of Mineralogy, Petrology and Geochemistry*, *35*, 1082–1089. https://doi.org/10.1007/s11430-017-9174-1

Guo, F., Fan, W. M., Gao, X. F., Li, C. W., Miao, L. C., Zhao, L., & Li, H. X. (2010). Sr–Nd–Pb isotope mapping of Mesozoic igneous rocks in NE China: Constraints on tectonic framework and Phanerozoic crustal growth. *Lithos*, *120*, 563–578. https://doi.org/10.1016/j.lithos.2010.09.020

Guo, F., Fan, W. M., Li, C. W., Miao, L. C., & Zhao, L. (2009). Early Paleozoic subduction of the Paleo-Asian Ocean: Geochronological and geochemical evidence from the Dashizhai basalts, Inner Mongolia. *Science in China, SeriesD-Earth Sciences*, *52*, 940–951. https://doi.org/10.1007/s11430-009-0083-2

Guo, F., Li, H. X., Fan, W. M., Li, J. Y., Zhao, L., Huang, M. W., & Xu, W. L. (2015). Early Jurassic subduction of the Paleo-Pacific Ocean in NE China: Petrologic and geochemical evidence from the Tumen mafic intrusive complex. *Lithos*, *224-225*, 46–60. https://doi.org/10.1016/j.lithos.2015.02.014

Handley, H. K., Macpherson, C. G., Davidson, J. P., Berlo, K., & Lowry, D. (2007). Constraining fluid and sediment contributions to subduction-related magmatism in Indonesia: Ijen Volcanic Complex. *Journal of Petrology*, *48*, 1155–1183. https://doi.org/10.1093/petrology/egm013

Handley, H. K., Simon, T., Macpherson, C. G., Gertisser, R., & Davidson, J. P. (2011). Hf–Nd isotope and trace element constraints on subduction inputs at island arcs: Limitations of Hf anomalies as sediment input indicators. *Earth and Planetary Science Letters*, *304*, 212–223. https://doi.org/10.1016/j.epsl.2011.01.034

Hanyu, T., Tatsumi, Y., Nakai, S., Chang, Q., Miyazaki, T., Sato, K., et al. (2006). Contribution of slab melting and slab dehydration to magmatism in the NE Japan arc for the last 25 Myr: Constraints from geochemistry. *Geochemistry, Geophysics, Geosystems*, *7*, Q08002. https://doi.org/10.1029/2005GC001220

Harry, D. L., & Green, N. L. (1999). Slab dehydration and basalt petrogenesis in subduction systems involving very young oceanic lithosphere. *Chemical Geology*, *160*(4), 309–333. https://doi.org/10.1016/S0009-2541(99)00105-9

Hawkesworth, C. J., Gallagher, K., Hergt, J. M., & McDermott, F. (1993). Mantle and slab contributions in arc magmas. *Annual Review of Earth and Planetary Sciences*, *21*(1), 175–204. https://doi.org/10.1146/annurev.ea.21.050193.001135

Hermann, J., & Spandler, C. J. (2008). Sediment melts at sub-arc depths: An experimental study. *Journal of Petrology*, *49*, 717–740. https://doi.org/10.1093/petrology/egm073

Hoang, N., Uto, K., Matsumoto, A., & Itoh, J. I. (2013). Pleistocene intraplate magmatism in the Goto Islands, SW Japan: Implications for mantle source evolution and regional geodynamics. *Journal of Geodynamics*, *68*, 1–17. https://doi.org/10.1016/j.jog.2013.03.002

Irvine, T. N., & Baragar, W. R. A. (1971). A guide to the chemical classification of the common volcanic rocks. *Canadian Journal of Earth Sciences*, *8*(5), 523–548. https://doi.org/10.1139/e71-055

James, D. E. (1981). The combined use of oxygen and radiogenic isotopes as indicatorsof crustal contamination. *Annual Review of Earth and Planetary Sciences*, *9*(1), 311–344. https://doi.org/10.1146/annurev.ea.09.050181.001523

Kessel, R., Schmidt, M. W., Ulmer, P., & Pettke, T. (2005). Trace element signature of subduction-zone fluids, melts and supercritical liquids at 120–180 km depth. *Nature*, *437*, 724–727. https://doi.org/10.1038/nature03971

Koppers, A. A. P., Morgan, J. P., Morgan, J. W., & Staudigel, H. (2001). Testing the fixed hotspot hypothesis using $^{40}Ar/^{39}Ar$ age progressions along seamount trails. *Earth and Planetary Science Letters*, *185*(3-4), 237–252. https://doi.org/10.1016/S0012-821X(00)00387-3

Li, C. Y., Zhang, H., Wang, F. Y., Liu, J. Q., Sun, Y. L., Hao, X. L., et al. (2012). The formation of the Dabaoshan porphyry molybdenum deposit induced by slab rollback. *Lithos*, *150*, 101–110. https://doi.org/10.1016/j.lithos.2012.04.001

Li, X. H., Abd El-Rahman, Y., Abu Anbar, M., Li, J., Ling, X. X., Wu, L. G., & Masoud, A. E. (2018). Old continental crust underlying juvenile oceanic arc: Evidence from northern Arabian-Nubian Shield, Egypt. *Geophysical Research Letters*, *45*, 3001–3008. https://doi.org/10.1002/2018GL077121

Li, X. H., Li, W. X., Li, Q. L., Wang, X. C., Liu, Y., & Yang, Y. H. (2010). Petrogenesis and tectonic significance of the 850 Ma Gangbian alkaline complex in South China: Evidence from in situ zircon U–Pb dating, Hf–O isotopes and whole-rock geochemistry. *Lithos*, *114*, 1–15. https://doi.org/10.1016/j.lithos.2009.07.011

Li, X. H., Li, Z. X., Wingate, M. T. D., Chung, S. L., Liu, Y., Lin, G. C., & Li, W. X. (2006). Geochemistry of the 755 Ma Mundine Well dyke swarm, northwestern Australia: Part of a Neoproterozoic mantle superplume beneath Rodinia? *Precambrian Research*, *146*, 1–15. https://doi.org/10.1016/j.precamres.2005.12.007

Liang, X. R., Wei, G. J., Li, X. H., & Liu, Y. (2003). Precise measurement of $^{143}Nd/^{144}Nd$ and Sm/Nd ratios using multiple collectors inductively coupled plasma mass spectrometer (MC-ICPMS) (in Chinese with English abstract). *Geochimica*, *32*, 91–96. https://doi.org/10.1007/s12303-013-0056-5

Lin, P. N. (1992). Trace element and isotopic characteristics of western Pacific pelagic sediments: Implications for the petrogenesis of Mariana Arc magmas. *Geochimica et Cosmochimica Acta*, *56*(4), 1641–1654. https://doi.org/10.1016/0016-7037(92)90231-7

Liu, K., Zhang, J. J., Wilde, S. A., Liu, S. R., Guo, F., Kasatkin, S. A., et al. (2017). U-Pb Dating and Lu-Hf Isotopes of Detrital Zircons from the Southern Sikhote-Alin Orogenic Belt, Russian Far East: Tectonic Implications for the Early Cretaceous Evolution of the Northwest Pacific Margin. *Tectonics*, *36*, 2555–2598. https://doi.org/10.1002/2017TC004599

Liu, K., Zhang, J. J., Wilde, S. A., Zhou, J. B., Wang, M., Ge, M. H., et al. (2017). Initial subduction of the Paleo-Pacific Oceanic plate in NE China: Constraints from whole-rock geochemistry and zircon U–Pb and Lu–Hf isotopes of the Khanka Lake granitoids. *Lithos*, *274-275*, 254–270. https://doi.org/10.1016/j.lithos.2016.12.022

Liu, Y. S., Gao, S., Hu, Z. C., Gao, C. G., Zong, K. Q., & Wang, D. B. (2010). Continental and oceanic crust recycling-induced melt-peridotite interactions in the trans-north China orogen: U–Pb dating, Hf isotopes and trace elements in zircons from mantle xenoliths. *Journal of Petrology*, *51*, 537–571. https://doi.org/10.1093/petrology/egp082

Liu, Y. S., Hu, Z. C., Gao, S., Gunther, D., Xu, J., Gao, C. G., & Chen, H. H. (2008). In situ analysis of major and trace elements of anhydrous minerals by LA-ICP-MS without applying an internal standard. *Chemical Geology*, *257*, 34–43. https://doi.org/10.1016/j.chemgeo.2008.08.004

Ludwig, K. R. (2003). Isoplot. In *A geochronological toolkit for Microsoft excelSpecial Publication* (pp. 1–70). Berkeley CA: Berkeley Geochronology Center.

Macdonald, R., Hawkesworth, C. J., & Heath, E. (2000). The Lesser Antilles volcanic chain: A study in arc magmatism. *Earth-Science Reviews*, *49*(1-4), 1–76. https://doi.org/10.1016/S0012-8252(99)00069-0

Manning, C. E. (2004). The chemistry of subduction-zone fluids. *Earth and Planetary Science Letters*, *223*, 1–16. https://doi.org/10.1016/j.epsl.2004.04.030

Marini, J. C., Chauvel, C., & Maury, R. C. (2005). Hf isotope compositions of northern Luzon arc lavas suggest involvement of pelagic sediments in their source. *Contributions to Mineralogy and Petrology*, *149*, 216–232. https://doi.org/10.1007/s00410-004-0645-4

Marschall, H. R., & Schumacher, J. C. (2012). Arc magmas sourced from mélange diapers subduction zones. *Nature Geoscience*, *5*, 862–867. https://doi.org/10.1038/ngeo1634

Maruyama, S., Liou, J. G., & Seno, T. (1989). Mesozoic and Cenozoic evolution of Asia. In Z. Ben-Avraham (Ed.), *The evolution of the Pacific Ocean margins* (pp. 75–99). New York: Oxford University Press.

McCulloch, M. T., & Gamble, J. A. (1991). Geochemical and geodynamical constraints on subduction zone magmatism. *Earth and Planetary Science Letters*, *102*(3-4), 358–374. https://doi.org/10.1016/0012-821X(91)90029-H

Meng, E., Xu, W. L., Pei, F. P., & Zhang, X. Z. (2011). Permian bimodal volcanism in the Zhangguangcai Range of eastern Heilongjiang Province, NE China: Zircon U–Pb–Hf isotopes and geochemical evidence. *Journal of Asian Earth Sciences*, *41*, 119–132. https://doi.org/10.1016/j.jseaes.2011.01.005

Miao, L. C., Fan, W. M., Liu, D. Y., Zhang, F. Q., Jian, P., Guo, F., et al. (2008). Geochronology and geochemistry of the Hegenshan ophiolitic complex: Implications for late-stage tectonic evolution of the Inner Mongolia-Daxinganling orogenic belt, China. *Journal of Asian Earth Sciences*, *32*, 348–370. https://doi.org/10.1016/j.jseaes.2007.11.005

Münker, C., Wörner, G., Yogodzinski, G., & Churikova, T. (2004). Behaviour of high field strength elements in subduction zones: Constraints from Kamchatka-Aleutian arc lavas. *Earth and Planetary Science Letters*, *224*, 275–293. https://doi.org/10.1016/j.epsl.2004.05.030

Nichols, G. T., Wyllie, P. J., & Stern, C. R. (1994). Subduction zone melting of pelagic sediments constrained by melting experiments. *Nature*, *371*(6500), 785–788. https://doi.org/10.1038/371785a0

Okamura, S., Inaba, M., Adachi, Y., & Shinjo, R. (2016). Miocene-Pliocene mantle depletion event in the northern Fossa Magna, western NE Japan. *Journal of Geodynamics*, *97*, 42–61. https://doi.org/10.1016/j.jog.2016.03.007

Pearce, J. A. (1983). Role of the sub-continental lithosphere in magma genesis at active continental margins. In C. J. Hawkesworth & M. J. Norry (Eds.), *Continental basalts and mantle xenoliths; Papers Prepared for a UK Volcanic Studies Group Meeting at the University of Leicester* (pp. 230–249). Nantwich: Shiva.

Pearce, J. A. (2014). Immobile element fingerprinting of ophiolites. *Elements*, *10*, 101–108. https://doi.org/10.2113/gselements.10.2.101

Pearce, J. A., Kempton, P. D., Nowell, G. M., & Noble, S. R. (1999). Hf-Nd element and isotope perspective on the nature and provenance of mantle and subduction components in Western Pacific arc-basin systems. *Journal of Petrology*, *40*(11), 1579–1611. https://doi.org/10.1093/petroj/40.11.1579

Pearce, J. A., & Peate, D. W. (1995). Tectonic implications of the composition of volcanic arc magmas. *Annual Review of Earth and Planetary Sciences*, *23*(1), 251–285. https://doi.org/10.1146/annurev.ea.23.050195.001343

Pearce, N. J. G., Perkins, W. T., Westgate, J. A., Gorton, M. P., Jackson, S. E., Neal, C. R., & Chenery, S. P. (1997). A compilation of new and published major and trace element data for NIST SRM 610 and NIST SRM 612 glass reference materials. *Geostandards Newsletter-The Journal of Geostandards and Geoanalysis*, *21*(1), 115–144. https://doi.org/10.1111/j.1751-908X.1997.tb00538.x

Pfänder, J. A., Jochum, K. P., Kozakov, I., Kröner, A., & Todt, W. (2002). Coupled evolution of back-arc and island arc-like mafic crust in the late-Neoproterozoic Agardagh Tes-Chem ophiolite, Central Asia: Evidence from trace element and Sr-Nd-Pb isotope data. *Contributions to Mineralogy and Petrology*, *143*(2), 154–174. https://doi.org/10.1007/s00410-001-0340-7

Plank, T. (2005). Constraints from thorium/lanthanum on sediment recycling at subduction zones and the evolution of the continents. *Journal of Petrology*, *46*, 921–944. https://doi.org/10.1093/petrology/egi005

Plank, T., Kelly, K. A., Murray, R. W., & Stern, L. Q. (2007). Chemical composition of sediments subducting at the Izu-Bonin trench. *Geochemistry, Geophysics, Geosystems*, *8*, Q04I16. https://doi.org/10.1029/2006GC001444

Plank, T., & Langmuir, C. H. (1993). Tracing trace elements from sediment input to volcanic output at subduction zones. *Nature*, *362*(6422), 739–743. https://doi.org/10.1038/362739a0

Plank, T., & Langmuir, C. H. (1998). The chemical composition of subducting sediment and its consequences for the crust and mantle. *Chemical Geology*, *145*(3-4), 325–394. https://doi.org/10.1016/S0009-2541(97)00150-2

Porritt, R. W., Miller, M. S., O'Driscoll, L. J., Harris, C. W., Roosmawati, N., & da Costa, L. T. (2016). Continent–arc collision in the Banda Arc imaged by ambient noise tomography. *Earth and Planetary Science Letters*, *449*, 246–258. https://doi.org/10.1016/j.epsl.2016.06.011

Portnyagin, M., Hoernle, K., Avdeiko, G., Hauff, F., Werner, R., Bindeman, I., et al. (2005). Transition from arc to oceanic magmatism at the Kamchatka-Aleutian junction. *Geology*, *33*(1), 25–28. https://doi.org/10.1130/G20853.1

Powell, R. (1984). Inversion of the assimilation and fractional crystallisation (AFC) equations: Suites. *Journal of the Geological Society*, *141*(3), 447–452. https://doi.org/10.1144/gsjgs.141.3.0447

Qi, L., Hu, J., & Gregoire, D. C. (2000). Determination of trace elements in granites by inductively coupled plasma mass spectrometry. *Talanta*, *51*(3), 507–513. https://doi.org/10.1016/S0039-9140(99)00318-5

Rapp, R. P., Irifune, T., Shimizu, N., Nishiyama, N., Norman, M. D., & Inoue, T. (2008). Subduction recycling of continental sediments and the origin of geochemically enriched reservoirs in the deep mantle. *Earth and Planetary Science Letters*, *271*, 14–23. https://doi.org/10.1016/j.epsl.2008.02.028

Richards, A., Argles, T., Harris, N., Parrish, R., Ahmad, T., Darbyshire, F., & Draganits, E. (2005). Himalayan architecture constrained by isotopic tracers from clastic sediments. *Earth and Planetary Science Letters*, *236*, 773–796. https://doi.org/10.1016/j.epsl.2005.05.034

Rudnick, R. L., & Gao, S. (2003). Composition of the continental crust. *Treatise on Geochemistry*, *3*, 1–64. https://doi.org/10.1016/B0-08-043751-6/03016-4

Scholl, D. W., & von Huene, R. (2007). Crustal recycling at modern subduction zones applied to the past—Issues of growth and preservation of continental basement crust, mantle geochemistry, and supercontinent reconstruction. In R. D. Hatcher, Jr., M. P. Carlson, J. H. McBride, & J. R. Martínez Catalán (Eds.), *4-D framework of continental crust* (Vol. 200, pp. 9–32). Geological Society of America Memoir. https://doi.org/10.1130/2007.1200(02)

Sengör, A. M. C., Natal'in, B. A., & Burtman, V. S. (1993). Evolution of the Altaid tectonic collage and Palaeozoic crustal growth in Eurasia. *Nature*, *364*(6435), 299–307. https://doi.org/10.1038/364299a0

Seton, M., Müller, R. D., Zahirovic, S., Gaina, C., Torsvik, T., Shephard, G., et al. (2012). Global continental and ocean basin reconstructions since 200 Ma. *Earth Science Reviews*, *113*, 212–270. https://doi.org/10.1016/j.earscirev.2012.03.002

Shao, J. A., & Tang, K. D. (1995). The Ophiolite Melange in Kaishantun, Jilin Province, China (in Chinese with English abstract). *Acta Petrologica Sinica*, *11*, 212–220.

Shimoda, G., Tatsumi, Y., Nohda, S., Ishizaka, K., & Jahn, B. M. (1998). Setouchi High-Mg andesites revisited: Geochemical evidence for melting of subducting sediments. *Earth and Planetary Science Letters*, *160*(3-4), 479–492. https://doi.org/10.1016/S0012-821X(98)00105-8

Shinjo, R., Chung, S. L., Kato, Y., & Kimura, M. (1999). Geochemical and Sr-Nd isotopic characteristics of volcanic rocks from the Okinawa Trough and Ryukyu Arc: Implications for the evolution of a young, intracontinental back arc basin. *Journal of Geophysical Research*, *104*(B5), 10,591–10,608. https://doi.org/10.1029/1999JB900040

Söderlund, U., Patchett, P. J., Vervoort, J. D., & Isachsen, C. E. (2004). The ^{176}Lu decay constant determined by Lu–Hf and U–Pb isotope systematics of Precambrian mafic intrusions. *Earth and Planetary Science Letters*, *219*(3-4), 311–324. https://doi.org/10.1016/S0012-821X(04)00012-3

Stolz, A., Jochum, K. P., Spettel, B., & Hofmann, A. W. (1996). Fluid- and melt-related enrichement in the subarc mantle: Evidence from Nb/Ta variations in island-arc basalts. *Geology*, *24*(7), 587–590. https://doi.org/10.1130/0091-7613(1996)024<0587:FAMREI>2.3.CO;2

Sun, M. D., Xu, Y. G., Wilde, S. A., Chen, H. L., & Yang, S. F. (2015). The Permian Dongfanghong island-arc gabbro of the Wandashan Orogen, NE China: Implications for Paleo-Pacific subduction. *Tectonophysics*, *659*, 122–136. https://doi.org/10.1016/j.tecto.2015.07.034

Sun, S. S., & McDonough, W. F. (1989). Chemical and isotopic systematics of oceanic basalts: Implications for mantle composition and processes. In A. D. Saunders & M. J. Norry (Eds.), *Magmatism in the ocean basinsSpecical Publication* (Vol. 42, pp. 315–345). Geological Society of London. https://doi.org/10.1144/GSL.SP.1989.042.01.19

Sun, W. D., Ding, X., Hu, Y. H., & Li, X. H. (2007). The golden transformation of the Cretaceous plate subduction in the west Pacific. *Earth and Planetary Science Letters*, *262*(3-4), 533–542. https://doi.org/10.1016/j.epsl.2007.08.021

Tang, G. Q., Li, X. H., Li, Q. L., Liu, Y., Ling, X. X., & Yin, Q. Z. (2015). Deciphering the physical mechanism of the topography effect for oxygen isotope measurements using a Cameca IMS-1280 SIMS. *Journal of Analytical Atomic Spectrometry*, *30*, 950–956. https://doi.org/10.1039/C4JA00458B

Tatsumi, Y., Hamilton, D. L., & Nesbitt, R. W. (1986). Chemical characteristics of fluid phase released from a subducted lithosphere and origin of arc magmas: Evidence from high-pressure experiments and natural rocks. *Journal of Volcanology and Geothermal Research*, *29*(1-4), 293–309. https://doi.org/10.1016/0377-0273(86)90049-1

Tatsumi, Y., & Kogiso, T. (2003). The subduction factory: Its role in the evolution of the Earth's crust and mantle. *Geological Society of London, Special Publication*, *219*(1), 55–80. https://doi.org/10.1144/GSL.SP.2003.219.01.03

Tollstrup, D. L., & Gill, J. B. (2005). Hafnium systematics of the Mariana arc: Evidence for sediment melt and residual phases. *Geology*, *33*(9), 737–740. https://doi.org/10.1130/G21639.1

Turner, S., Handler, M., Bindeman, I., & Suzuki, K. (2009). New insights into the origin of O–Hf–Os isotope signatures in arc lavas from Tonga-Kermadec. *Chemical Geology*, *266*(3-4), 187–193. https://doi.org/10.1016/j.chemgeo.2009.05.027

Valley, J. W. (2003). Oxygen isotopes in zircon. In J. M. Hanchar & P. W. O. Hoskin (Eds.), *ZirconReviews in Mineralogy and Geochemistry* (Vol. 53, pp. 343–385). Washington, DC: Mineralogical Society, of America.

Valley, J. W., Lackey, J. S., Cavosie, A. J., Clechenko, C. C., Spicuzza, M. J., Basei, M. A. S., et al. (2005). 4.4 billion years of crustal maturation: Oxygen isotope ratios of magmatic zircon. *Contributions to Mineralogy and Petrology*, *150*(6), 561–580. https://doi.org/10.1007/s00410-005-0025-8

van de Flierdt, T., Goldstein, S. L., Hemming, S. R., Roy, M., Frank, M., & Halliday, A. N. (2007). Global neodymium-hafnium isotope systematics—Revised. *Earth and Planetary Science Letters*, *259*(3-4), 432–441. https://doi.org/10.1016/j.epsl.2007.05.003

Vervoort, J. D., Blichert-Toft, J., Patchett, P. J., & Albarede, F. (1999). Relationships between Lu–Hf and Sm–Nd isotopic systems in the global sedimentary system. *Earth and Planetary Science Letters*, *168*(1-2), 79–99. https://doi.org/10.1016/S0012-821X(99)00047-3

Vervoort, J. D., Plank, T., & Prytulak, J. (2011). The Hf–Nd isotopic composition of marine sediments. *Geochimica et Cosmochimica Acta*, *75*, 5903–5926. https://doi.org/10.1016/j.gca.2011.07.046

Walowski, W. J., Wallace, P. J., Clynne, M. A., Rasmussen, D. J., & Weis, D. (2016). Slab melting and magma formation beneath the southern Cascade arc. *Earth and Planetary Science Letters*, *446*, 100–112. https://doi.org/10.1016/j.epsl.2016.03.044

Wang, F., Xu, W. L., Ge, W. C., Yang, H., Pei, F. P., & Wu, W. (2016). The offset distance of the Dunhua-Mishan Fault: Constraints from Paleozoic-Mesozoic magmatism within the Songnen-Zhangguangcai Range, Jiamusi, and Khanka massifs (in Chinese with English abstract). *Acta Petrologica Sinica*, *61*, 527–559. https://doi.org/10.1007/s11430-017-9174-1

Wang, F., Xu, W. L., Xu, Y. G., Gao, F. H., & Ge, W. C. (2015). Late Triassic bimodal igneous rocks in eastern Heilongjiang Province, NE China: Implications for the initiation of subduction of the Paleo-Pacific Plate beneath Eurasia. *Journal of Asian Earth Sciences*, *97*, 406–423. https://doi.org/10.1016/j.jseaes.2014.05.025

Wang, Z. W., Pei, F. P., Xu, W. L., Cao, H. H., Wang, Z. J., & Zhang, Y. (2016). Tectonic evolution of the eastern Central Asian Orogenic Belt: Evidence from zircon U–Pb–Hf isotopes and geochemistry of early Paleozoic rocks in Yanbian region, NE China. *Gondwana Research*, *38*, 334–350. https://doi.org/10.1016/j.gr.2016.01.004

Wedepohl, K. H. (1995). The composition of the continental crust. *Geochimica et Cosmochimica Acta*, *59*(7), 1217–1232. https://doi.org/10.1016/0016-7037(95)00038-2

Wei, G. J., Liang, X. R., Li, X. H., & Liu, Y. (2002). Precise measurement of Sr isotopic composition of liquid and solid base using (LP) MC-ICPMS (in Chinese with English abstract). *Geochimica*, *31*, 295–299.

Weis, D., Kieffer, B., Maerschalk, C., Pretorius, W., & Barling, J. (2005). High-precision Pb-Sr-Nd-Hf isotopic characterization of USGS BHVO-1 and BHVO-2 reference materials. *Geochemistry, Geophysics, Geosystems*, *6*, Q02002. https://doi.org/10.1029/2004GC000852

Whitney, D. L., & Evans, B. W. (2010). Abbreviations for names of rock-forming minerals. *American Mineralogist*, *95*, 185–187. https://doi.org/10.2138/am.2010.3371

Wiedenbeck, M., Hanchar, J. M., Peck, W. H., Sylvester, P., Valley, J., Whitehouse, M., et al. (2004). Further characterisation of the 91500 zircon crystal. *Geostandards and Geoanalytical Research*, *28*, 9–39. https://doi.org/10.1111/j.1751-908X.2004.tb01041.x

Windley, B. F., Alexeiev, D. V., Xiao, W. J., Kröner, A., & Badarch, G. (2007). Tectonic models for accretion of the Central Asian Orogenic Belt. *Journal of the Geological Society, London*, *164*, 31–47. https://doi.org/10.1144/0016-76492006-022

Wood, D. A. (1980). The application of a Th-Hf-Ta diagram to problems of tectonomagmatic classification and to establishing the nature of crustal contamination of basaltic lavas of the British Tertiary Volcanic Province. *Earth and Planetary Science Letters*, *50*(1), 11–30. https://doi.org/10.1016/0012-821X(80)90116-8

Woodhead, J. D. (1989). Geochemistry of the Mariana arc (western Pacific): Source composition and processes. *Chemical Geology*, *76*(1-2), 1–24. https://doi.org/10.1016/0009-2541(89)90124-1

Woodhead, J. D., Hergt, J. M., Davidson, J. P., & Eggins, S. M. (2001). Hafnium isotope evidence for 'conservative' element mobility during subduction zone processes. *Earth and Planetary Science Letters*, *192*(3), 331–346. https://doi.org/10.1016/S0012-821X(01)00453-8

Workman, R. K., & Hart, S. R. (2005). Major and trace element composition of the depleted MORB mantle (DMM). *Earth and Planetary Science Letters*, *231*, 53–72. https://doi.org/10.1016/j.epsl.2004.12.005

Wu, F. Y., Jahn, B. M., Wilde, S., & Sun, D. Y. (2000). Phanerozoic crustal growth: U–Pb and Sr–Nd isotopic evidence from the granites in northeastern China. *Tectonophysics*, *328*(1-2), 89–113. https://doi.org/10.1016/S0040-1951(00)00179-7

Wu, F. Y., Jahn, B. M., Wilde, S. A., Lo, C. H., Yui, T. F., Lin, Q., et al. (2003). Highly fractionated I-type granites in NE China (II): Isotopic geochemistry and implications for crustal growth in the Phanerozoic. *Lithos*, *67*(3-4), 191–204. https://doi.org/10.1016/S0024-4937(03)00015-X

Wu, F. Y., Sun, D. Y., Ge, W. C., Zhang, Y. B., Grant, M. L., Wilde, S. A., & Jahn, B. M. (2011). Geochronology of the Phanerozoic granitoids in northeastern China. *Journal of Asian Earth Sciences*, *41*, 1–30. https://doi.org/10.1016/j.jseaes.2010.11.014

Wu, F. Y., Sun, D. Y., Li, H. M., Jahn, B. M., & Wilde, S. A. (2002). A-type granites in northeastern China: Age and geochemical constraints on their petrogenesis. *Chemical Geology*, *187*(1-2), 143–173. https://doi.org/10.1016/S0009-2541(02)00018-9

Wu, F. Y., Yang, J. H., Lo, C. H., Wilde, S. A., Sun, D. Y., & Jahn, B. M. (2007). The Heilongjiang group: A Jurassic accretionary complex in the Jiamusi rat the western Pacific margin of northeastern China. *Island Arc*, *16*, 156–172. https://doi.org/10.1111/j.1440-1738.2007.00564.x

Wu, F. Y., Yang, Y. H., Xie, L. W., Yang, J. H., & Xu, P. (2006). Hf isotopic compositions of the standard zircons and baddeleyites used in U-Pb geochronology. *Chemical Geology*, *234*, 105–126. https://doi.org/10.1016/j.chemgeo.2006.05.003

Xiao, W. J., Windley, B. F., Hao, J., & Zhai, M. G. (2003). Accretion leading to collision and the Permian Solonker suture, Inner Mongolia, China: Termination of the central Asian orogenic belt. *Tectonics*, *22*(6), 1069. https://doi.org/10.1029/2002TC001484

Xu, B., Zhao, P., Wang, Y. Y., Liao, W., Luo, Z. W., Bao, Q. Z., & Zhou, Y. H. (2015). The pre-Devonian tectonic framework of Xing'an–Mongolia orogenic belt (XMOB) in north China. *Journal of Asian Earth Sciences*, *97*, 183–196. https://doi.org/10.1016/j.jseaes.2014.07.020

Xu, J. W., Zhu, G., Tong, W. X., Cui, K., & Liu, Q. (1987). Formation and evolution of the Tancheng-Lujiang wrench fault system: A major shear system to the northwest of the Pacific Ocean. *Tectonophysics*, *134*(4), 273–310. https://doi.org/10.1016/0040-1951(87)90342-8

Xu, W. L., Pei, F. P., Wang, F., Meng, E., Ji, W. Q., Yang, D. B., & Wang, W. (2013). Spatial–temporal relationships of Mesozoic volcanic rocks in NE China: Constraints on tectonic overprinting and transformations between multiple tectonic regimes. *Journal of Asian Earth Sciences*, *74*, 167–193. https://doi.org/10.1016/j.jseaes.2013.04.003

Yu, J. J., Wang, F., Xu, W. L., Gao, F. H., & Pei, F. P. (2012). Early Jurassic mafic magmatism in the Lesser Xing'an–Zhangguangcai Range, NE China, and its tectonic implications: Constraints from zircon U–Pb chronology and geochemistry. *Lithos*, *142-143*, 256–266. https://doi.org/10.1016/j.lithos.2012.03.016

Zhang, Y. B., Wu, F. Y., Wilde, S. A., Zhai, M. G., Lu, X. P., & Sun, D. Y. (2004). Zircon U–Pb ages and tectonic implications of "Early Paleozoic" granitoids at Yanbian, Jilin Province, northeast China. *Island Arc*, *13*(4), 484–505. https://doi.org/10.1111/j.1440-1738.2004.00442.x

Zhang, Y. Q., Dong, S. W., & Shi, W. (2003). Cretaceous deformation histroy of the middle Tan-Lu fault zones in Shandong Province, eastern China. *Tectonophysics*, *363*(3-4), 243–258. https://doi.org/10.1016/S0040-1951(03)00039-8

Zhou, J. B., Cao, J. L., Wilde, S. A., Zhao, G. C., Zhang, J. J., & Wang, B. (2014). Paleo-Pacific subduction-accretion: Evidence from geochemical and U–Pb zircon dating of the Nadanhada accretionary complex, NE China. *Tectonics*, *33*, 2444–2466. https://doi.org/10.1002/2014TC003637

Zhou, J. B., & Li, L. (2017). The Mesozoic accretionary complex in Northeast China: Evidence for the accretion history of Paleo-Pacific subduction. *Journal of Asian Earth Sciences*, *145*, 91–100. https://doi.org/10.1016/j.jseaes.2017.04.013

Zhou, J. B., & Wilde, S. A. (2013). The crustal accretion history and tectonic evolution of the NE China segment of the Central Asian Orogenic Belt. *Gondwana Research*, *23*, 1365–1377. https://doi.org/10.1016/j.gr.2012.05.012

Zhou, J. B., Wilde, S. A., Zhang, X. Z., Zhao, G. C., Zheng, C. Q., Wang, Y. J., & Zhang, X. H. (2009). The onset of Pacific margin accretion in NE China: Evidence from the Heilongjiang high-pressure metamorphic belt. *Tectonophysics*, *478*, 230–246. https://doi.org/10.1016/j.tecto.2009.08.009